Optimization of Particle Size of α-Alumina Separator on Performance of Lithium Ion Batteries

by

Narayan Kanhere

A Thesis Presented in Partial Fulfillment
of the Requirements for the Degree
Master of Science

Approved April 2017 by the
Graduate Supervisory Committee:

Jerry Y.S. Lin, Chair
Candace Chan
Arunachala Kannan

ARIZONA STATE UNIVERSITY

August 2017

ABSTRACT

Lithium ion batteries prepared with a ceramic separator, have proven to possess improved safety, reliability as well as performance characteristics when compared to those with polymer separators which are prone to thermal runaway. Purely inorganic separators are highly brittle and expensive. The electrode-supported ceramic separator permits thinner separators which are a lot more flexible in comparison. In this work, it was observed that not any α-alumina could be used by the blade coating process to get a good quality separator on $Li_4Ti_5O_{12}$ (LTO) electrode. In this work specifically, the effect of particle size of α-alumina, on processability of slurry was investigated. The effect of the particle size variations on quality of separator formation was also studied. Most importantly, the effect of alumina particle size and its distribution on the performance of LTO/Li half cells is examined in detail. Large-sized particles were found to severely limit the ability to fabricate such separators. The α-alumina slurry was coated onto electrode substrate, leading to possible interaction between α-alumina and LTO substrate. The interaction between submicron sized particles of α-alumina with the substrate electrode pores, was found to affect the performance and the stability of the separator. Utilizing a bimodal distribution of submicron sized particles with micron sized particles of α-alumina to prepare the separator, improved cell performance was observed. Yet only a specific ratio of bimodal distribution achieved good results both in terms of separator formation and resulting cell performance. The interaction of α-alumina and binder in the separator, and its effect on the performance of substrate electrode was investigated, to understand the need for bimodal distribution of powder forming the separator.

Dedicated to my parents,

Vishnu and Sujata Kanhere

and my sister,

Gayatri Kanhere

ACKNOWLEDGMENTS

I would like to thank my advisor, Dr. Jerry Y.S. Lin for giving me this great opportunity to work on the exciting and developing area of lithium ion batteries. I am grateful for his support, guidance and inspiration. I am thankful for his trust and belief in my abilities. His constant motivation, encouragement and the freedom to work independently, gave me the confidence to push towards excellence. His deep involvement in my projects was crucial in maintaining the pace of work. I am blessed to have him as my mentor and guide, from whom I have learnt the importance of hard work and perseverance in research and also the value of punctuality, discipline and work ethics. I thank Dr. Lin for steering my career path in the right direction.

I would like to thank Dr. Arunachala Kannan and Dr. Candace Chan for kindly agreeing to serve on my committee. As faculty for my courses on Batteries and Electrochemistry, I learnt the basics required for my research from them. Their expertise and knowledge helped me a lot in this project. I appreciate their recommendations and valuable feedback.

I would also like to thank Fred Pena for promptly helping in fixing equipment issues in the lab. Without his help, a lot of valuable research time would have been lost.

I would like to thank all the current and former members of Dr. Lin's group from whom I learnt a great deal. It was an absolute pleasure to work alongside such a talented group of people: Dr. Linghui Yu, Dr. Zebao Rui, Dr. Chien-Hua Chen, Dr. Lie Meng, Dr. Liang-Chih Ma, Dr. Sainan Liu, Dr. Margarita Judith Ramirez, Joshua James, Amr Ibrahim, Jiansong Miao, Han-Chun Wu, Oscar Ovalles Encinia, Suzanne Williams, Fateme Benihashemi, Gaurav Sharma, Iordan Iordanov and Paul McAfee.

I would also like to specially thank Jason for helping me with the SEM imaging of my samples, Amr for helping me with FTIR of my samples, Oscar for helping me with nitrogen porosity, Ben for teaching me the particle size distribution calculation technique and Josh for countless number of times that I have bothered him and he has gladly helped me.

I would also like to thank, Dr. Lenore Dai and Dr. Nikhilesh Chawla and their students for allowing me to carry out mechanical testing in their laboratory. I would like to thank China Electric Power Research Institute (CEPRI) for their financial support to this project. I would also like to thank Celgard for providing PP polymer separators for this research. I would also like to thank Sumitomo and Aluchem respectively for providing alumina powders for this research.

I am grateful to my parents for their support and encouragement throughout my life. Their constant belief in me has enabled me to pursue my dream. I am also grateful to my grandmother for her blessings and encouragement.

TABLE OF CONTENTS

Page

LIST OF TABLES

LIST OF FIGURES

Figure Page

CHAPTER 1

INTRODUCTION

1.1 Overview

Lithium ion batteries (LIB) for energy storage applications, have found a wide acceptance due to their better characteristics. LIBs are known to possess high energy density, elevated cell voltage, great cyclability and long shelf life. [1] They are found extensively in electronic portable devices as well as electric vehicles. As of recently, LIBs are being sought after as an intermediary energy storage solution for renewable energy applications. Wind and solar energy generated is being stored via LIBs for later use. [2] LIBs are a class of secondary batteries. The major components of a LIBs are a negative electrode or anode, a positive electrode or cathode and a Lithium ion conducting electrolyte. LIB electrode materials are selected, based on the criteria that they should permit intercalation of the lithium ions. This means, the lithium ions can be inserted and extracted reversibly into the crystal structures of these electrode materials. The most commonly used anode material is Graphite. Lithium Titanium Oxide (LTO) is a relatively newer material that has also garnered a lot of interest due to its zero-strain nature and low voltage gap between discharge and charge step. While the most commonly used cathode material is Lithium Cobalt Oxide ($LiCoO_2$). Other popular cathode materials employed include Lithium Manganese Oxide ($LiMn_2O_4$), Lithium Iron Phosphate ($LiFePO_4$) and Lithium Nickel Cobalt Oxide ($LiNi_{0.85}Co_{0.15}O_2$).

The electrolytes employed in LIBs are usually a lithium salt prepared with organic solvents to form a non-aqueous solution. The reason for avoiding aqueous electrolytes is that LIBs operate at a voltage much greater than the voltage at which water electrolyzes

(1.23 V). Instead organic solvents such as ethylene carbonate (EC), propylene carbonate (PC), diethyl carbonate (DEC), tetrahydro furan (THF), dimethyl carbonate (DMC), are commonly used. These organic solvents are mixed in varying ratios to suit the intended cell application, as each solvent has different properties. The organic solvents are used are non-conductive of lithium ions. Hence, inorganic Lithium salts are dissolved in these organic solvents to conduct lithium ions. Lithium hexaflourophosphate ($LiPF_6$) is most commonly used due to its exceptionally high conductivity. Lithium perchlorate ($LiClO_4$), Lithium tetrafluoroborate ($LiBF_4$) and LiBOB ($LiBC_4O$) are also used as inorganic Lithium salts in LIB electrolytes.

As lithium ion batteries are commonly used for portable applications, there is a requirement for LIBs to be compact in nature. At the same time, LIBs should be capable of providing a high energy density with minimal internal resistance. In an ideal case to achieve this, we would need to place the electrodes as close to one another as physically possible but without bringing them in actual contact. Due to the LIB assembly considerations, this is not possible as the cells are based in a liquid electrolyte and the two electrodes will come into direct contact if assembled as is. Thus leading to a short-circuit. To prevent thermal runaway or shorting of the electrodes, LIBs employ separators to keep the electrodes apart and avoid electrical contact between the two electrodes.

Taking separators into consideration, LIBs should seek to use good separators. A good separator should have the following properties. The separator should have a high porosity and good wettability towards the non-aqueous electrolyte used in LIBs. This ensures good absorption of electrolyte within the separator, leading to high lithium ion conduction. However, as the separator is an electrically inactive component, therefore it

should be as thin as physically possible. This limits the ohmic component of resistance in the cell. The separator is also required to be physically stable and cannot disintegrate during assembly or life cycle of the cell. Hence, the separator material chosen should also be chemically non-reactive with the other cell components. To ensure stability and safety of the LIB the separator should be capable of withstanding extreme cell conditions as well.

1.2 Literature Review

The separators in LIB are an integral part associated with the proper functioning of the cells. The polymeric separators just do not possess the desired qualities to serve as all round high quality failsafe separators in the LIB. To address the various limitations posed by the polymeric separators, inorganic materials have been studied as a possible option. [3] Inorganic materials such as alumina (Al_2O_3) and silica (SiO_2) inherently possess a highly hydrophilic nature making them an excellent choice for use with almost all the non-aqueous electrolytes. [4], [5] Apart from good wettability, they demonstrate an improved mechanical integrity even at elevated temperatures owing to their ceramic nature.

Polymeric separators are very often coated with ceramic powders due to the advantages offered by ceramic materials. These ceramic coated separators exhibit a better wettability towards electrolyte as well as reduced shrinkage at a higher temperature. [6] For a coated polymeric separator, the ceramic content is usually low, with the polymer composing the major chunk of the separator material. [3] For a 25-30 µm polymeric separator, the ceramic content coated is usually not more than a third of the thickness. The combustibility of such coated separators is still a significant cause of concern. Therefore,

these inorganic coated separators are not immune to high temperature effects and can still lead to thermal runaway. On the other hand, ceramic coated polymeric separators offer comparatively improved characteristics but cannot completely overcome material property issues faced by the polymeric separators due to their high polymer content. This shifts the focus towards free-standing ceramic separators. Thus, attempts were made to fabricate separators with reduced or minimal polymer content.

Zhang et al [7] utilized $CaCO_3$ with Teflon only as a binder, in an emulsion to prepare a free-standing ceramic separator. As these separators contained a high ceramic content, greater stability at elevated temperatures and an increase in wettability by the electrolyte was reported. While at the same time it addresses the issue of flammability of the separator owing to its ceramic content. Standalone ceramic separators are very brittle and cost intensive to manufacture. [8] A purely inorganic separator was reported by Xiang et al. [9] Al_2O_3 was used to prepare the standalone wholly ceramic separator. A two-step sintering process was employed to achieve the final separator. Pore formation using EDTA as pore former, was conducted by sintering at a temperature of 1000 ^oC. To obtain better mechanical stability in the final separator, the samples were treated for 5 hours at 1500 ^oC. A high porosity was reported for these separators. Better wettability by the electrolyte also permitted higher ionic conductivity. Yet a major challenge was that the process of sintering is very energy intensive and thus makes it expensive to manufacture such separators on a large scale. A solution to these issues reported in the literature has been to prepare electrode supported separators.

The various issues posed by free-standing purely inorganic separators such as poor mechanical integrity and highly cost intensive processing needed to be addressed.

Some work has been directed to tackling these issues in the recent years. A review of the various methods attempted and the key takeaway from each work is discussed ahead.

An alumina membrane on anode with a thickness of 60 μm, was reported as a separator by Chen et al. [10] The separator for an LIB formed by a two-step anodization process, forming uniform open-hole structure with >70% porosity was reported. The high porosity and excellent wettability of the anodic alumina separator also ensured good rate-capability and good low temperature performance of the LIBs that were assembled. He et al. [11] reported using alumina nanowires to prepare ∼50 μm flexible mesh separator. An aluminum based precursor was pressurized at an elevated temperature via hydrothermal treatment to fabricate these membranes. The amount of nanowire used was adjusted to achieve desired thickness control. Although these separators reported by Chen et al. and He et al., were both prepared without any polymeric content, eliminating even the binder, yet the fabrication processes involved are sufficiently complex, chemically exhaustive and significantly expensive.

Purely inorganic standalone separators have been investigated, and the issues pertaining to brittleness and cost of manufacture due to energy intensive steps such as sintering could not be overcome while maintaining the same setup. In contrast, Kim et al [12] reported the use of alumina powder for the first time, to prepare anode coated separators. A suspension of 600 nm sized alumina particles with PVDF-HFP in acetone was used and a dip-coating process was reported to prepare the separators. Dip-coating time of the electrode in the suspension was kept at 1 s. A drying step followed with a time of 5 min. Control over membrane thickness was achieved by varying solid contents in suspension. Thickness control was of about 8-25 μm was reported. The assembled

cells demonstrated good cyclability and thermal stability. Dip-coating affects the ease of manufacture and scalability. Commercially electrode materials are blade coated in slurry form, onto a substrate current collector. [13] This makes blade coating of separator materials on the electrode, lucrative for LIB manufacturers due to ease of manufacture and scalability.

On similar lines, Mi et al [14] reported an alumina separator which was directly blade coated on lithium titanium oxide (LTO) electrode. The ceramic separators reported in their work are easy to manufacture and more flexible than standalone ceramic separators reported previously. Rather than using a dip-coating process and an alumina suspension, Mi et al. reported using alumina slurry based in water which was prepared by a much simpler blade coating process. This, as a water based slurry makes the drying step quicker. The quality of the coating is improved due to the use of alumina as slurry rather than suspension. ~ 50 µm thin electrode supported ceramic separators were successfully prepared in their findings. The performance of LIB half cells prepared with the reported electrode coated alumina separator is comparable to LIB half cells prepared with commercial polymer separators. These separators exhibited improved thermal stability and assembled cells demonstrated an improved rate capability.

A two-step blade coating process reported by Sharma et al [15] lead to thinner (upto ~30 µm), much more stable, electrode coated alumina separators. The ability of coating the ceramic alumina separator on a variety of commercial electrodes was illustrated. Low and high temperature performance of the cells assembled with the separator was also reported. Unlike polymeric separators, a wide range of electrolytes were able to wet the separator. Additionally, a higher capacity retention was

demonstrated for the ceramic separators cells. These separators exhibited the desired mechanical property of almost no shrinkage at elevated temperatures.

All these works have extensively dealt with thermal stability, and improved electrochemical performance of cells with alumina based electrode coated separators. However, none of these works present any insight regarding the effect of alumina powder selection on the quality of the separator achieved. In the literature, there is no information available regarding the effects of particle size of the selected ceramic powder on the separator formation or performance.

1.3 Statement of the problem

Lithium ion batteries suffer a major drawback due to the safety consideration. A relatively high number of cases of lithium ion battery initiated fires and explosions have been reported in the past many years. Lithium ion batteries are very prone to thermal runaway issues. [16] The flammable organic solvents used in the electrolyte combined with the polymeric separator involved in fabrication of LIBs, are the primary cause for this. Polymeric separators have low melting points, and are flammable in nature leading to a serious problem. At raised temperatures, the polymer based separators show a tendency to shrink and melt, causing the electrodes to electrically short under certain specific conditions. Such instances of shorting may occur due to overcharging or external damage which are responsible for thermal runaway in the cells. The combustibility of LIB cell components makes thermal runaway dangerous. [17]

Almost all commercial lithium-ion battery systems currently manufactured, are utilizing liquid electrolytes. Therefore, wettability of the separator by a wide range of electrolytes, is an important requirement. The polymeric materials used in commercial

LIBs as separators such as polypropylene (PP) and polyethylene (PE) show poor wettability towards the electrolytes due to their surface characteristics. The poor wettability leads to poor electrolyte retention and thus affects cyclability of the battery. Poor wettability also results in more wetting time required for each separator, thus increasing production time of each cell. This ends up reducing the cost effectiveness of the manufacturing process, indicating a need for change in the separator material.

While evolved separators reported and used more recently, which are purely ceramic in nature face the issues of poor mechanical robustness and being very thick, which reduces the total energy density per unit weight of the cell. This lead to development of electrode coated ceramic separators. Through this work, it was observed that not every ceramic material proves successful in assembling LIBs. Thus, the need to have a detailed study on the nature of the ceramic and its effect at each step of manufacture, assembly and cell performance is required.

1.4 Objectives of research and thesis structure

Although previous work by Mi et al. [14], studies the functioning of the coated alumina separator, the focus of the work was on the ability of the separator to form stable LIBs. While work by Sharma et al. [15] primarily focuses on the properties of alumina separator at extreme temperatures. Both works were successful only in using a bimodal alumina powder as separator in LIB. It is therefore correct to assume that alumina particle size possibly affects quality of separator formation and thus assembled cell performance. In both these works, only one specific alumina powder of micron size particles with a few submicron size particles was successfully utilized to prepare the separator.

It is therefore hypothesized that a bimodal mixture of particles leads to superior slurry properties due to the appropriate capillary force exerted by the particles of two different size ranges upon the liquid component of the slurry. Submicron sized particles should not permit formation of a good separator by this method of fabrication. This proposition is a valid consideration as submicron sized particles are smaller than the pore size of the substrate electrode, and a mechanical coating method would lead to blocking of electrode pores due to physical entry of these particles into such pores. Hence as the quantity of submicron particles in this separator is increased, corresponding reduction in electrode performance should be observed. On the other hand, purely micron sized particles should be difficult to synthesize into a well bound slurry. A larger particle size implies lower capillary force and liquid content of slurry might flow into electrode pores rather than being held together by the alumina particles.

The objective of this research work is to validate the above hypothesis by investigating the effect of α-alumina particle size on the various modules involved in the fabrication of a separator that gives good cell performance. In this work, a study of various grades of α-alumina powder is conducted. The effect of the nature of α-alumina particles on the slurry formation properties is investigated. Not all α-alumina powders are capable of forming consistent slurries as was seen from initial work. Further, the α-alumina slurries that can be used by the blade coating process are also limited. Theoretically due to difference in particle size, not every α-alumina that can be prepared into separators, will show the exact same mechanical property and dimensional integrity. As the particle size varies one would expect to see a variation in the observed separator quality.

In this work, the electrode material used is Lithium Titanium Oxide (LTO). LTO is also inorganic in nature. Hence, there could be possible interactions between the particles of α-alumina based separator and underlying substrate electrode. Through this work, we expect to obtain a better understanding of the effect of particle size-distribution of α-alumina on slurry formation, separator fabrication and cell performance. Hence determining the optimum particle size distribution of α-alumina in a ceramic separator, to achieve to achieve best possible LIB performance.

CHAPTER 2

OPTIMIZATION OF INORGANIC SEPARATOR FOR LITHIUM ION BATTERIES

2.1 Introduction

As discussed in Chapter 2, Mi et al. [14] demonstrated the feasibility of coating a slurry of alumina powder on the LTO electrode as a separator for LIBs. Improved thermal stability of the separator in comparison to the commercial PP separator was proven. However, the reported separator was > 60 μm in thickness. While Gaurav et al [15] reported an improved method to produce such separators with a thickness as low as 40 μm. As mentioned before, both these works have established the thermal stability, mechanical integrity and high temperature performance capabilities of this separator.

But both these works used an α-alumina composed of particles of the size of a few microns with a small percentage of submicron sized particles. They did not address the issue of variations in separator fabrication or cell performance with change in the type of alumina being used in the fabrication process. In this work, particle size effects of alumina will be studied in detail. The interaction of α-alumina particles with substrate LTO electrode is also examined.

2.2 Experiments

2.2.1 Preparation and characterization of coated ceramic separator

Ceramic separators were fabricated by a two-step blade coating process, using a slurry of commercially produced α-Al_2O_3 powder. Varying particle sizes of α-Al_2O_3 powder were used. Not all the α-Al_2O_3 powders formed a consistent slurry, and few others despite forming a consistent slurry, did not permit separator formation by blade

coating process. Hence, Table 2.2.1 summarizes the types of α-Al_2O_3 powders studied and their respective characteristics.

In Figure 2.2.1, particle size distribution data is provided in graphical form for two α-Al_2O_3 powders. Particle size distribution was calculated on the basis of numerical occurrences of a given particle size from the SEM images of the separator samples. Detailed method for this calculation is provided in Appendix A. A similar volume based calculation was also conducted but since volume contribution of the submicron sized particles is low, a numerical approach was used to indicate presence of submicron sized particles.

Table 2.2.1: α-alumina powders investigated in this study

	Powder used	Reference Code	Manufacturer	Particle Size (microns)	Consistent slurry formation	Uniform separator formation
1	A13	VL1	Alcoa	**50-100**	No	No
2	A10325	L1	Alcoa	**5-15**	Yes	No
3	A14325	L2	Alcoa	**1-10**	Yes	No
4	AC12	BD1	Aluchem	**0.2-6**	Yes	Yes
5	A2750	BD2	Alcoa	**1-4**	Yes	Yes
6	A17	BD3	Alcoa	**0.2-4**	Yes	Yes
7	AA3	M1	Sumitomo	**3**	Yes	Yes
8	AKP-30	N1	Sumitomo	**0.27**	Yes	Yes
9	AKP-15	N2	Sumitomo	**0.6**	Yes	Yes

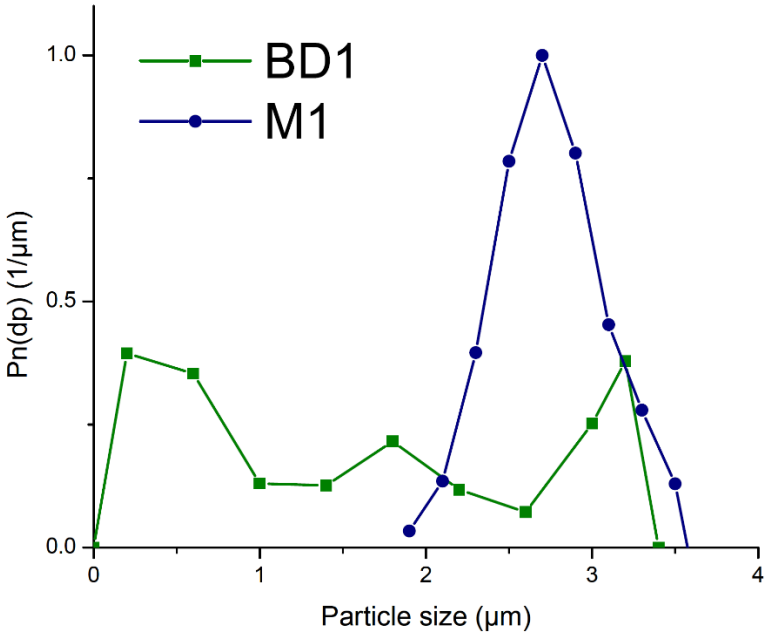

Figure 2.2.1: Particle size distribution curves for M1 and BD1 powders respectively

By adding 10 g of an α-alumina powder to 2.2 – 4.2 g of deionized H_2O and mixing with 0.8-1.4 g of 5 wt% PVA binder (average M.W. of 77000-79000) (ICN Biomedicals, Inc.), the slurry was prepared. Prepared slurry composition varied and was specific to each α-alumina powder. The details of the slurry compositions are provided respectively in Table 2.2.2 and Table 2.2.3. Table 2.2.2 details slurry compositions for commercially obtained alumina powders, while Table 2.2.3 details slurry compositions for the alumina powders that were prepared into a simulated mixture.

Table 2.2.2 : Slurry composition and coating speed for α-aluminas

	Powder used as separator	Particle Size (microns)	Alumina : PVA : Water (% wt)	Coating Speed
1	BD1	**3** (0.2-6)	69.4 : 0.3 : 30.3	Medium
2	BD2	**1-4**	69.4 : 0.3 : 30.3	Medium
3	BD3	**0.2-5**	69.4 : 0.3 : 30.3	Medium
4	M1	**3**	73.5 : 0.5 : 26	Fast
5	N1	**0.27**	66.7 : 0.3 : 33	Slow
6	N2	**0.6**	67.5 : 0.3 : 32.2	Slow

Table 2.2.3: Simulated mixtures of α-alumina powders

	Powder used as separator	Particle Size (microns)	Alumina : PVA : Water
1	SM (M1 : N2 = 90:10)	**0.6, 3**	73.5 : 0.5 : 26
2	SM2 (M1 : N2 = 80:20)	**0.6, 3**	73.5 : 0.5 : 26
3	SM3 (M1 : N2 = 30:70)	**0.6, 3**	73.5 : 0.5 : 26

The slurry thus prepared was stirred thoroughly for a period of at least 30 minutes. The purpose of stirring the slurry was to remove any aggregates that may form. This leads to achievement of a uniform slurry consistency. Using $Li_4Ti_5O_{12}$ (LTO) electrode as substrate material, the fully prepared α-alumina slurry was coated onto it. Composition of LTO electrode (CEPRI, Beijing, China) is, 90 wt% of LTO, with 5 wt% of PVDF as binder and 5 wt% of carbon black coated on current collector of Aluminum foil. The LTO electrode density was 8.5 mg/cm^2. 70 µm thickness of LTO electrode material with a total density of 90 g/cm^2 was coated on an aluminum foil which was 18 µm thick.

The simulated powders listed in Table 2.2.3 were prepared from commercially available alumina powders. A micron sized powder M1 was selected to be mixed with

submicron sized powder N2. These two powders were selected due to the uniformity in their unimodality. The two powders were mixed physically on a purely measured weight % basis. These powders were mixed in varying ratios to obtain slurries and separators which were tested by assembling the separators into LIB coin cells. Powder compositions and uniformity were confirmed with SEM imaging.

Doctor blade (Digital II Micrometer Film Applicator) (Gardco LLC, Pompano Beach, FL), was used to coat the homogenous slurry onto the surface of LTO electrode substrate. The blade gap was used in order to adjust the thickness of applied separator material. Manipulating the calipers, the blade gap on the doctor blade device could be adjusted. Determination of thickness of the coating layer applied, was done with micrometer caliper (Mitutoyo Corp., USA). The micrometer calipers were accurate within 1 μm. All samples were kept to dry at 40 C for 12h, post the preparation of each coated alumina layer, in a humidity-controlled chamber. Relative humidity of the drying chamber was controlled at 60%. The purpose of keeping the prepared separator samples to dry in a humidity chamber is to reduce drying rate so that separator layer does not crack during drying.

Using a disc cutter (Compact & Precision Disc Cutter with Standard 16 mm Diameter Cutting Die, MSK-T-10) (MTI, Richmond, CA) prepared coated α-Al_2O_3 separators were cut into discs of 16 mm diameter. The cut disks were kept to dry for 12 h in a vacuum oven at a temperature of 70 ^{o}C. The final LTO samples coated with prepared separator are subjected to the vacuum heating step to remove any water content that may still be present in the samples from the fabrication step. At this point, the alumina coated LTO electrode was ready for assembly. As a performance reference for α-alumina based

cells, the commercial porous PP separator (PP2500) (Celgard LLC,Charlotte, NC) was also studied in this work.

By using a scanning electron microscopy (SEM, Philips FEI XL-30) the morphologies of the coated Al_2O_3 separators were characterized. As alumina is non conductive, the samples were gold-coated prior to insertion into the SEM chamber. Figure 2.2.2 represents a typical alumina separator coated on LTO and its surface morphology. A simple porosity calculation was conducted by collecting the measured weight, and measured geometric dimensions to obtain volume of alumina coated part of the sample. Using the theoretical density ($\rho_{alumina}$ = 3.9 g cm^{-3}) for coated alumina layer, porosity was calculated and is reported in Table 2.3.3. The results of the simplified porosity calculation were cross-confirmed using a non-destructive liquid nitrogen method for porosity determination.

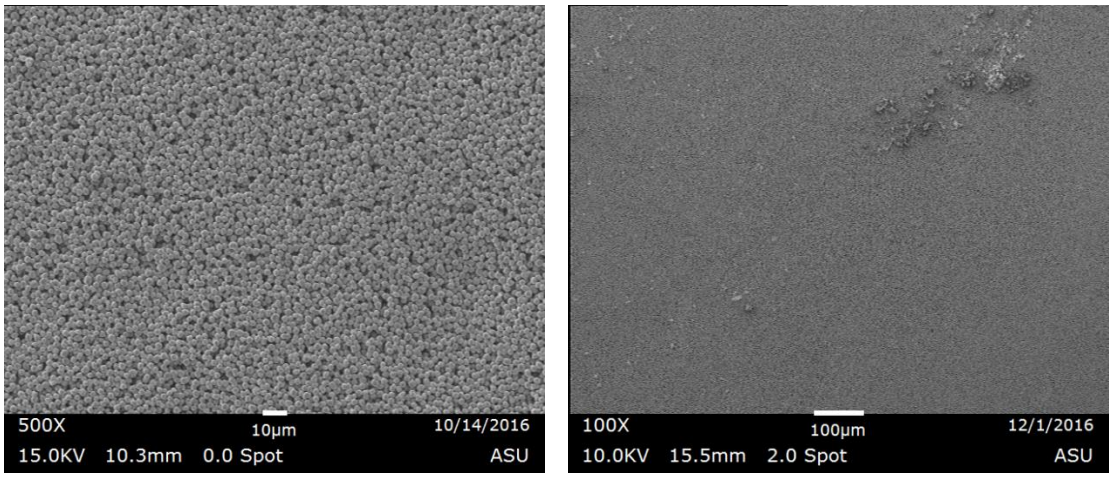

Figure 2.2.2 : SEM of the surface of a typical Alumina coated LTO electrode showing quality of separator layer

The method involves suspending the Al_2O_3 coated aluminum foil by a string from a support, which is placed on the weighing scale. A dewar of liquid nitrogen is placed at the bottom of this setup, which is positioned on a surface that can be adjusted to move up

or down. This permits the sample to be immersed in and removed from the liquid nitrogen by manipulating the position of the liquid nitrogen dewar. This is a completely rudimentary setup which is prepared manually.

The dry weight of the sample is recorded as D. Upon submerging the sample in liquid nitrogen, it is kept submerged for a short time (few seconds) to ensure all the pores have been filled. Upon stabilization of the weight reading, this is confirmed. Submerged sample saturated weight is recorded. The weight of the saturated sample when weighed in air is noted as W. However, liquid nitrogen proceeds to evaporate as the sample is being removed from the liquid nitrogen containing dewar. The saturated weight denoted as S, is calculated by measuring weight loss at 5 s intervals. This provides a linear relation for time versus weight loss. As a result, the saturated weight can be obtained by extrapolating the weight of the sample at time t = 0. [18] This leads to observed variations in the results of porosity measurement by this method. However, the results are reproducible and only minor error observed in the values is represented in the Table 2.3.3 along with the actual calculated values. Porosity formula is given as follows.

$$P\,\% = \frac{W - D}{W - S} * 100$$

The electrolyte uptake and retention of the many separators was tested by using the method most commonly used in LIB literature. [19]:

$$Electrolyte\ Uptake = \frac{w1 - \ w0}{w0} * 100\ \%$$

$$Electrolyte\ Retention = \frac{wx - \ w0}{w1 - w0} * 100\ \%$$

where Wo is the weight of dry separator, W1 is the weight of the separator after absorbing the electrolyte for 1 h. Wx is the equilibrium weight of the electrolyte-

infiltrated separator treated at 50 °C at varying intervals of time. Any excess electrolyte was first drawn off with a filter paper. Parallel measurements were carried out for different separators under the identical conditions and three individual sets of data measurements per separator material were also conducted.

2.2.2 Cell assembly and electrochemical measurements

For studying the electrochemical performance of many different separator samples, CR2032 coin cells were assembled. In all the assembled the coin cells, 70 µm thick LTO on aluminum foil was the cathode used. While the anode that was used was lithium metal chips (MTI, Richmond, CA). The lithium metal chips are 0.1 mm in thickness with 15.6 mm as diameter. A solution of 1M LiPF6 salt in equal volume of ethyl carbonate (EC), diethyl carbonate (DEC) and dimethyl carbonate (DMC) (EC:DEC:DMC ¼ 1:1:1, v/v/v) (MTI, Richmond, CA) was used as electrolyte. Argon filled glove box (Innovative Technology Inc, Amesbury, MA), was used as an inert atmosphere to assemble the coin cells. The contents of oxygen and water vapor were kept below 0.5 ppm within the glovebox.

For a typical cell, the LTO coated with alumina separator, was cut into a disc of 16 mm diameter, and placed within a CR2032 negative case. Electrolyte was then filled into the coated alumina layer. A lithium metal chip was then gently placed down on the cell contents. Two spacers and a spring were added to the cell. The positive plate of the cell was placed on top. Using a coin cell crimper (MSK-110) (MTI, Richard, CA) the cell was sealed. LTO active material content of about 20 mg was present in each cell.

NEWARE Battery Testing System (BTS3000) (Neware Co, China) was used to conduct charge-discharge cycling of the assembled half cells. With a typical CC-CV

(Constant Current-Constant Voltage, constant current density) method of cycling, the cells were cycled between 1 - 2.5 V. Using PARSTAT 2263 EIS station (Princeton Applied Research, Oak Ridge, TN) in DC mode, Electrochemical Impedance Spectroscopy measurements were carried out for the assembled cells. Setting a frequency range of 100 kHz to 100 mHz, the Nyquist plots for assembled Li/LTO half cells were generated. EIS data was successfully curve fitted using the open source software (EC lab). Thus, for different components of the cells, the resistance values were obtained and noted. A simplistic and standard lithium cell models was applied for the fitting.

2.3 RESULTS AND DISCUSSION

2.3.1 Synthesis of α-alumina slurries

By coating the slurry of α-alumina (BD3) onto electrode substrate, the coated α-alumina separator was prepared by Mi et al. [14]. With PVA as a binder, the α-alumina slurry is based in water and must be of homogenous and consistent characteristics. Water is preferred in the slurry over commonly used N-methyl pyrrolidone (NMP). The reason for avoiding NMP is that it is toxic and expensive. [20] Additional data regarding the properties of formed slurry used in this work is provided in Table 2.3.2. In this table, pH of the various slurries at varying compositions is provided.

The formed slurry is also required to have a moderately high viscosity to coat well on the substrate. A wide variety of powders were examined for the purpose of slurry preparation in this study. The slurry preparation study results are listed in Table 2.2.1. From the work of Sharma et. al [15], it is known that VL1 demonstrated a high tendency towards froth formation as well as sedimentation.

As can be seen in Figure 2.3.1, a very frothy slurry was obtained and could not be used as it was not homogenous at all even after thorough stirring of the prepared slurry. Upon applying the slurry to electrode surface, the solids would settle and adhere to the surface while the bubbles from the froth would lead to uncovered surface on the electrode. It was possible to form consistent slurries out of all the other α-alumina powders. The various grades of α-alumina that were studied are listed under Table 2.2.2. Comments on the slurry composition, its nature and properties and its effect on consistent slurry formation are also briefly mentioned in the tabulated data.

First, a detailed study of the slurry preparation was conducted. The α-alumina powders were prepared into slurries at varying water contents with a fixed binder content as reference. However, the aim was to form as viscous slurries as possible, yet maintain homogeneity. The results of this study are put forth and explained below.

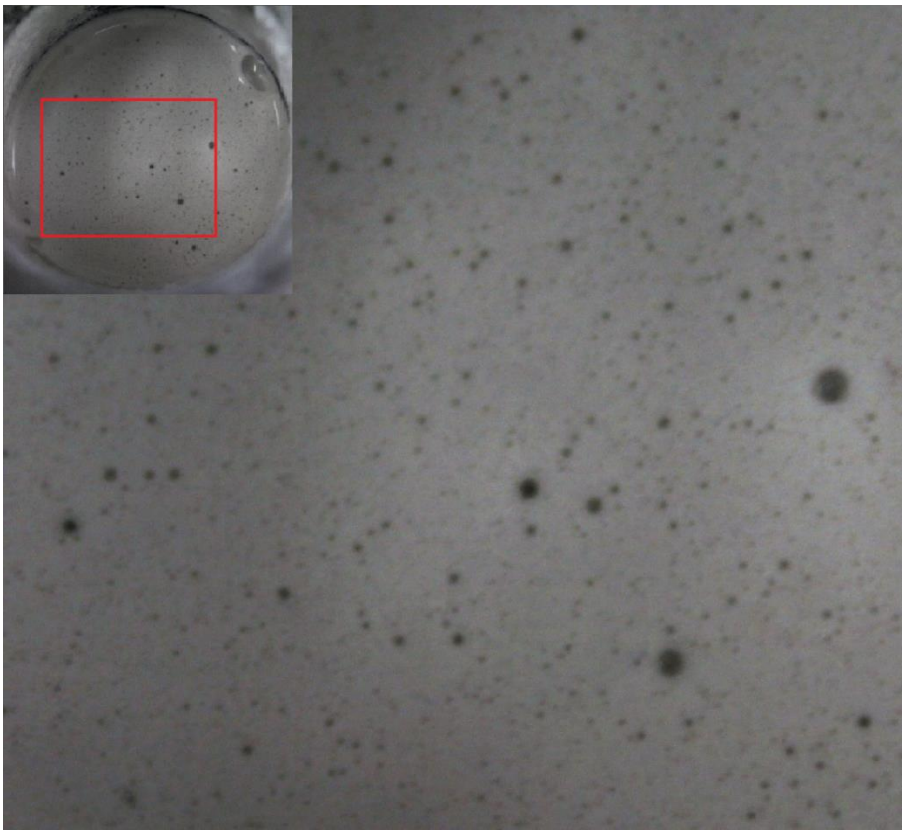

Figure 2.3.1 : Non homogenous froth forming slurry of VL1. Original image of slurry in the beaker. (inset)

The submicron sized powders (N1, N2) displayed a highly viscous nature in slurry form. While the micron sized powder (M1) displayed very low viscous nature in the slurry form. Powders with the bimodal distribution of both submicron sized and micron sized particles (BD1, BD2, BD3), display similar viscosity in formed slurry. Variation in formed slurry viscosity was observed. In Figure 2.3.2, this variation is qualitatively presented. On an inclined surface, an equal volume of the 3 slurries in water

- N1, M1 and BD1 respectively, were placed near the top edge of the surface. The top edge for placement of the slurry was marked with a line and downward arrow. After time t=100s an image was captured for each N1 (Figure 2.3.2a), BD1 (Figure 2.3.2b) and M1 (Figure 2.3.2c) respectively. The varying rate of flow between the different slurries can be attributed to varying viscosities of three slurries leading to different length of flow along the inclined plane, respectively. The viscosity of the three slurries, can be concluded from Figure 2.3.2, are in the following order, from least to most – M1, BD1 and N1.

Table 2.3.1 : pH analysis of various slurries and slurry components

Slurry composition	Weight Ratios	pH
M1 : PVA : water	5 : 0.7 : 1.1	6.3
M1 : water	5 : 1.1	7.1
BD1 : PVA : water	5 : 0.4 : 1.8	8.5
BD1 : water	5 : 1.8	8.9
N1 : PVA : water	5 : 0.4 : 2.2	8.0
N1 : water	5 : 2.2	8.3
PVA : water	1 : 0	4.2
PVA : water	5 : 1.1	5.7
PVA : water	5 : 1.8	6.1

In table 2.3.1, the pH values are listed for the various slurries and components of the slurries. While there is no direct correlation between particle size and pH, nor is there a direct correlation between pH and coating ability of the slurry. On the other hand a correlation between particle size and viscosity was observed. It should be noted that, the only slurry that leads to poorly adhering coat on the electrode is the slurry M1. M1 without PVA has an almost neutral pH and in combination with PVA gives a pH less than 7. While all other slurries have a final pH value greater than 7. This might explain why M1 slurry does not adhere as well to substrate electrode.

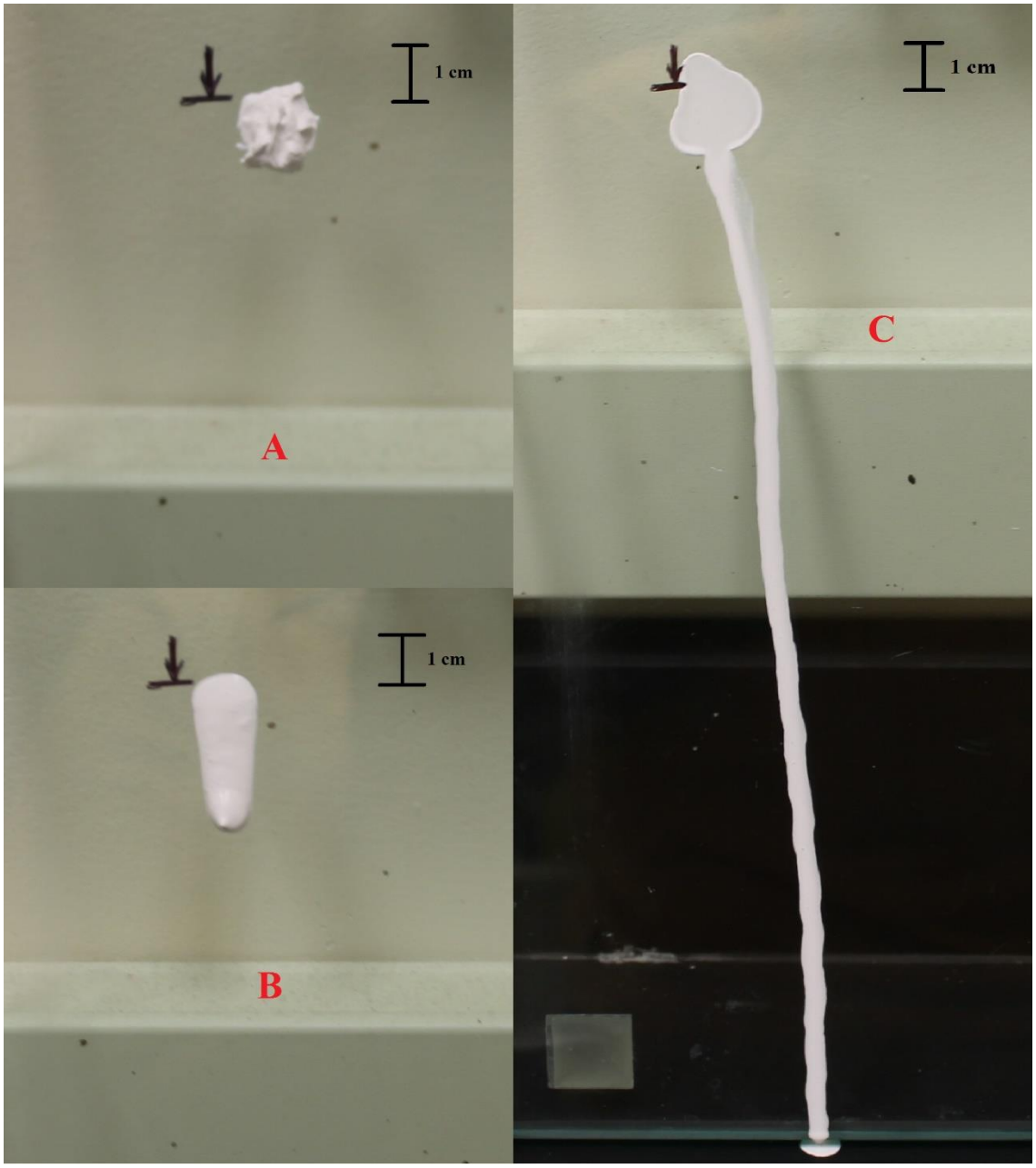

Figure 2.3.2 : a] Slurry N1 did not flow at all along inclined surface upto t=100s. **b] :** Slurry BD1 flowed a small distance from the top margin, along inclined surface upto t=100s. **c] :** Slurry M1 flows almost rapidly along the inclined surface upto t=100s.

Only an α-alumina that is incapable of undergoing any kind of aggregation, froth formation or sedimentation should be utilized for this blade coating process. It is observed that α-alumina powders with a mean particle size larger than 20 μm, tend to

undergo sedimentation when formed into a slurry, as the particles are heavy. [15] A major observation was the variation in observed viscosity based on particle size of α-alumina used during the preparation of the different alumina slurries.

For a smaller mean particle size observed viscosity was higher as was the case with the unimodal submicron sized α-alumina powders which demonstrate a very high viscosity when formed into a water based slurry. On the other hand the significantly larger unimodal α-alumina particles of micron size exhibit a much lower viscosity in slurry form, comparatively. Ideal viscosity for blade coating was obtained using the powders with bimodal distribution of α-alumina particles. Thus explaining a trend with respect to particle size and slurry formation.

2.3.2 Synthesis of α-alumina separators

α-alumina powder slurry based in water was used via the two-step blade coating process for coating α-alumina separator layer on LTO electrode substrate. Only the alumina VL1 failed to form a consistent slurry and could not be used for the blade coating process. L1 and L2 powders both completely failed to coat onto the electrode material. This is illustrated through the observation made in figure 2.3.3. When blade coating of the alumina slurries of L1 and L2 respectively was attempted, there was no adherence of the slurry to the substrate at all. [15]. All the other powders that could form homogenous slurries coated considerably well onto the electrode surface.

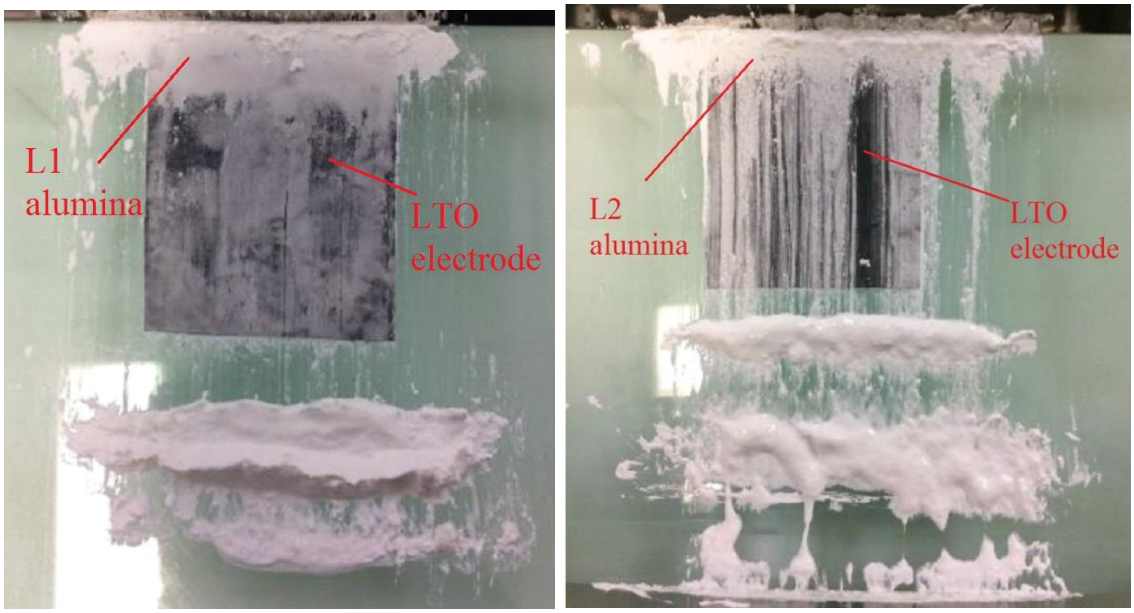

Figure 2.3.3 : L1 (left) and L2 (right) slurries failed to coat on the LTO electrode substrate [15]

LTO electrode substrate exhibits a hydrophilic surface. To confirm the hydrophilicity, a contact angle measurement was conducted and can be seen in Figure 2.3.4. A contact angle of < 90 was observed for the substrate LTO electrode. Micron sized alumina M1 was coated onto LTO substrate. The coating speed was varied to study the effect and relation of coating speed with viscosity. The results from varying the coating velocity can be observed in Figure 2.3.5.

In the Figure 2.3.5a, at a higher coating speed, the slurry failed to adhere to the substrate. In Figure 2.3.5b, at a moderate coating speed, a good quality coat was obtained. In Figure 2.3.5c, when the highly reduced coating speed was used, it lead to poor coating ability with visible damage to the electrode substrate most likely due to absorption of water at various points from the slurry. To get a better understanding of coating speed relation to viscosity, a similar study for the highly viscous slurry of submicron sized powder N1 was conducted as well. At a higher coating velocity, the slurry failed to coat

(Figure 2.3.6a). On the other hand, at lower velocity of coating, the alumina particles coated well due to better adherence. (Figure 2.3.6b).

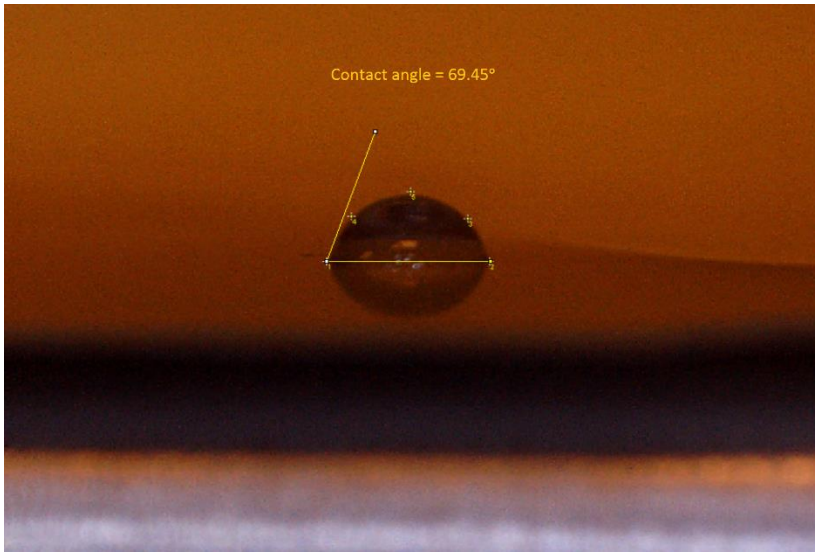

Figure 2.3.4: LTO contact angle measurement (hydrophilic)

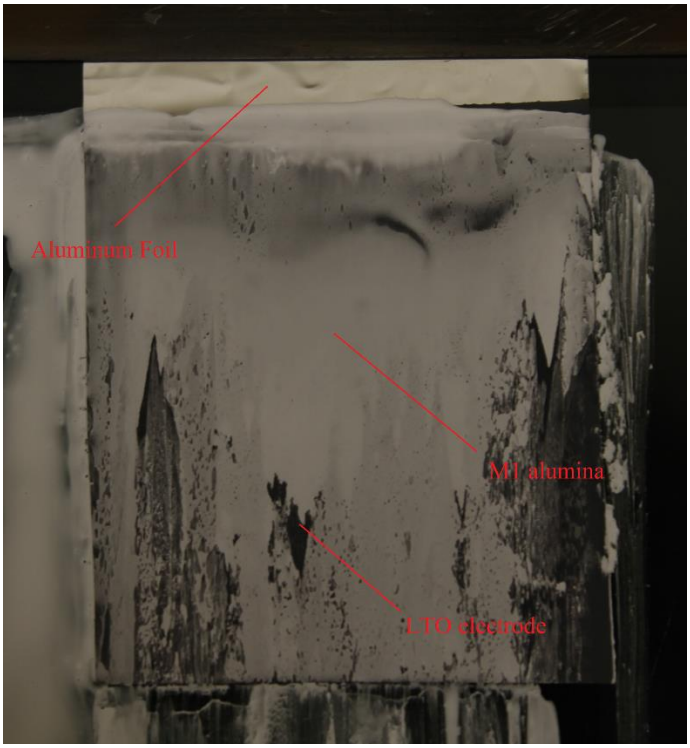

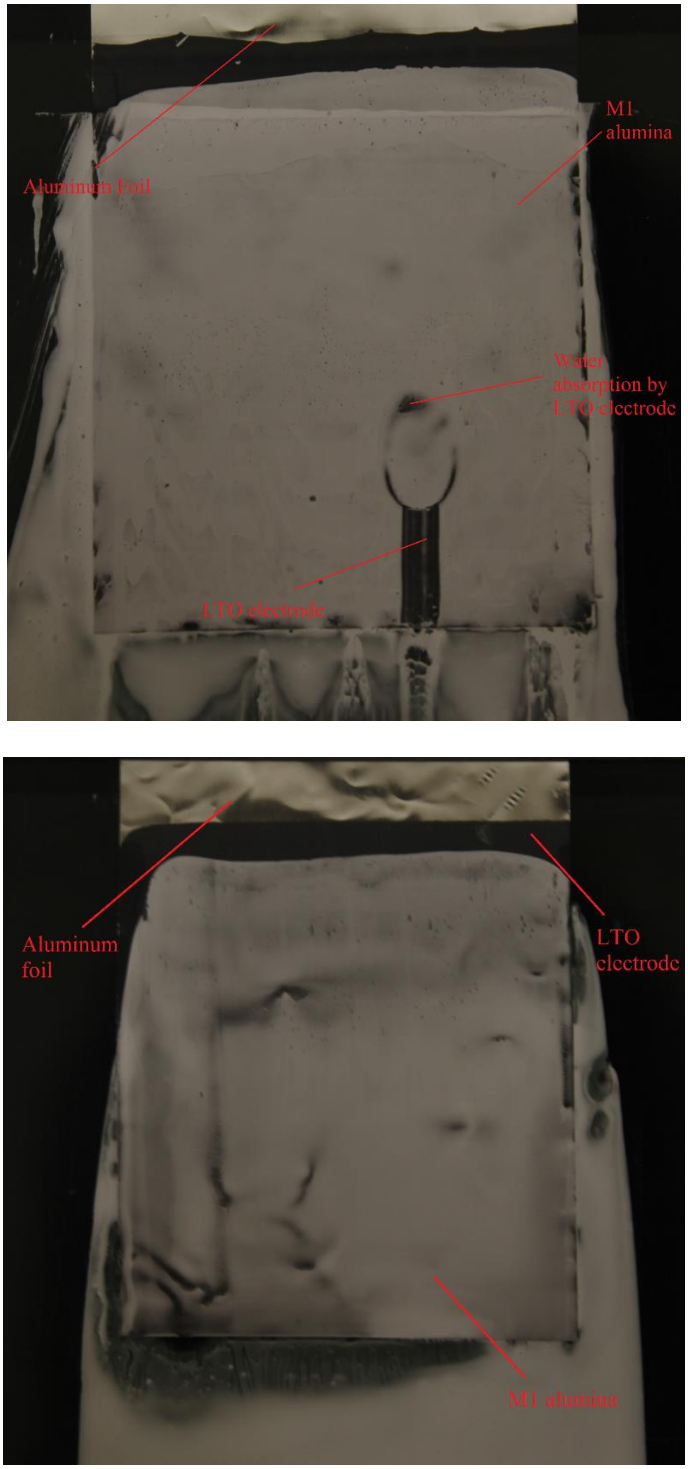

Figure 2.3.5: (Clockwise) a] Very rapid coating speed for M1 slurry, poor adherence, bad quality coat observed. b] Very slow coating speed for M1 slurry, water damage from slurry affecting coating of the electrode. c] At moderate coating speed, good quality coat achieved.

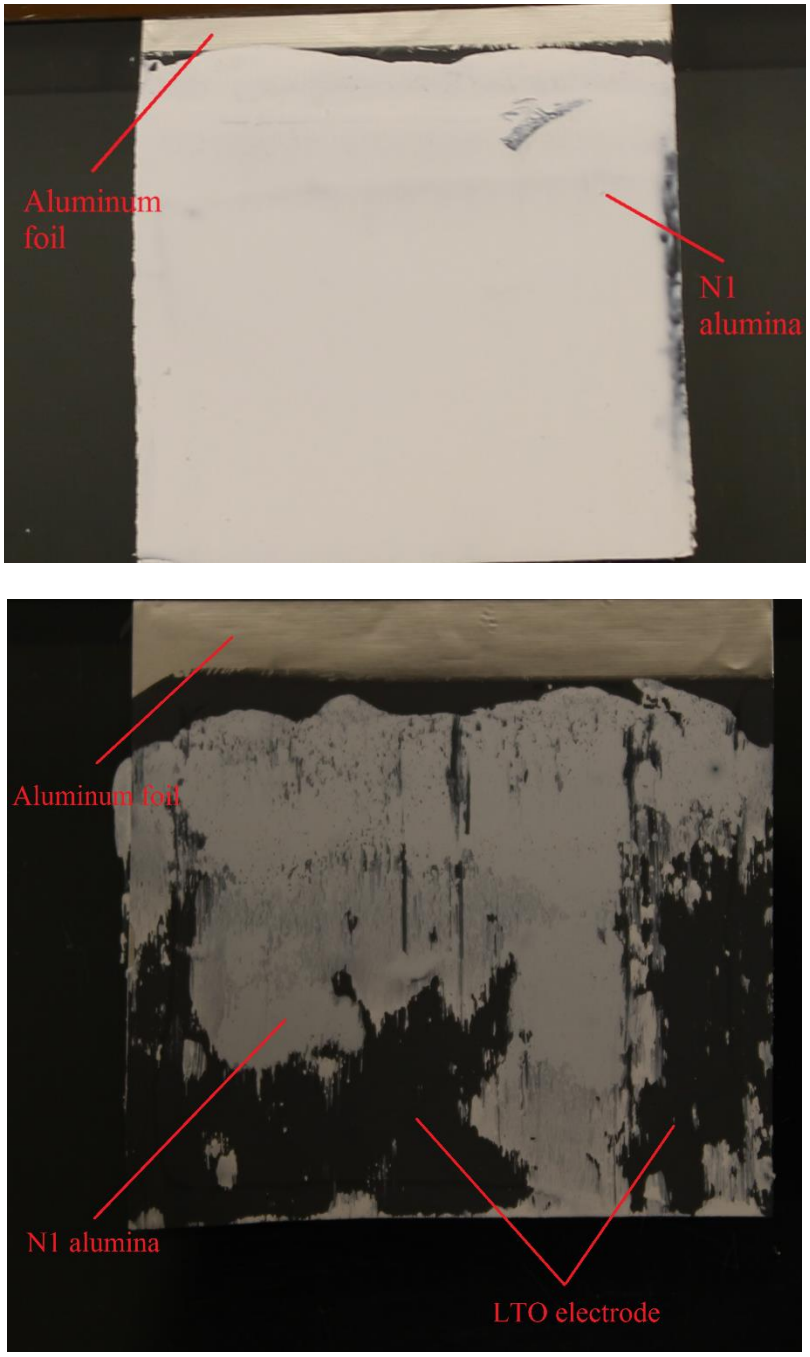

Figure 2.3.6 : a] (top) N1 slurry coated at high velocity, poor adherence, separator layer not formed. b] (bottom) N1 slurry coated at lower velocity, good coat obtained.

During the process of slurry coating and separator formation, the powders BD 1-3, N1-2 and M1, ended up forming a separator of uniform thickness respectively on the substrate

electrode. M1 formed a separator that was significantly more brittle and the layer was more loosely bound and poorly adhered to the electrode. BD1 and M1 coated separator samples were folded along the middle of the sample to illustrate this finding. Figure 2.3.7 shows the completely opposite adhering ability of the two formed separators. On folding the separator samples, micron sized M1 separator caked off without any difficulty and there was no visible change to be observed for the separator of BD1. This would suggest a different interaction between particles of M1, PVA binder and the substrate as compared to that of all other aluminas studied in this work.

Table 2.3.2 quantifies approximately the values of coating speed summarized for the observations from Figure 2.3.5 and Figure 2.3.6. Another analysis of the slurries was conducted by measuring the pH values of the three slurries of N1, M1 and BD1 with and without PVA content, as well that for different concentrations of PVA solution. The results are tabulated in Table 2.3.1.

Table 2.3.2 : Quantitative representation of coating speed variations

Slurry	Coating speed (quantitative)	Coating speed (qualitative)
M1	3.33 cm/s	Fast
M1	1.56 cm/s	Moderate
M1	0.82 cm/s	Slow
N1	2.94 cm/s	Fast
N1	1.22 cm/s	Moderate to slow

To better convey the changes in the quality of formed separator, a simulation of powder mixtures was attempted. The ratios of micron to sub-micron sized particles of α-alumina were modified in the different mixtures. The simulated powders are presented in Table 2.2.3. An improved mechanical stability and integrity of coated alumina layer was observed when M1 powder was prepared by mixing it in the different ratios of submicron sized particles.

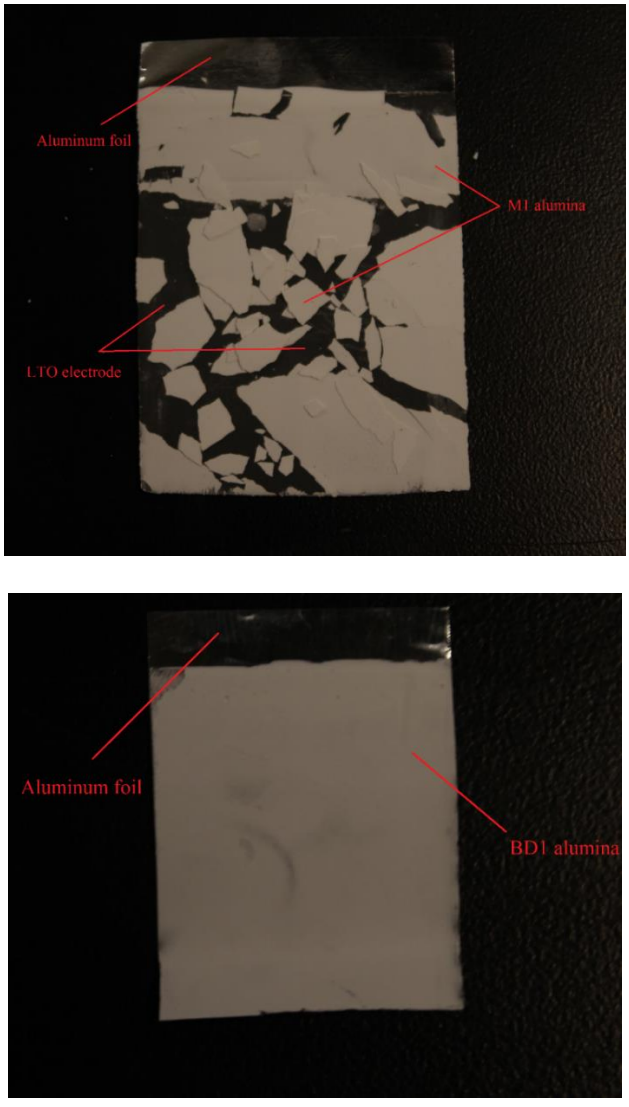

Figure 2.3.7: Separator stability : M1 separator cakes off upon folding the sample (top), BD2 separator shows no visible damage upon folding. (bottom)

The high shear force could be the primary reason behind the inability of the large particle size powders to coat. Blade gap of ~ 15-25 µm was used and this was very close to the actual mean particle size of the powder. To avoid such negative shear force effect during blade coating, the usable α-alumina powders, are reduced to a particle size range of approximately 7 µm and lower in this study.

For high slurry viscosity, coating velocity must be slower, to allow better contact between the surfaces of α-alumina particles and the electrode material. This leads to good binding of α-alumina particles to the underlying electrode. Therefore, resulting in a highly uniform and continuous separator layer. Although, if the slurry viscosity is somewhat significantly low, it is observed that the interaction time between slurry and electrode should be kept as short as possible. This suggests that, the LTO substrate being highly hydrophilic, it tends to absorb water rapidly from the slurry. This ends up affecting coat quality as well as electrode performance. Therefore, coating speed is a variable that must be monitored to achieve a uniform separator layer on LTO. The coating speed does not play much of a role if the slurry was to be coated directly onto a current collector as the substrate is not hydrophilic. A uniform separator layer formed on LTO substrate v/s that formed on current collector are almost similar in terms of structure and integrity.

To characterize the formed separators, the same procedure for separator formation was used to coat the α-alumina layer on aluminum foil instead of LTO electrode as substrate. Although the structure of the separator may vary when coated on aluminum foil v/s LTO electrode, this is the most practical way to study conduct porosity calculations. As well as to study electrolyte uptake and retention properties of the separator material by itself. In Table 2.3.3, the porosity values for the various separators are provided.

The porosity of all the separators happens to be more than that of the polymeric separator. Except for the ones containing unimodal micron size powder M1. However, as particles of M1 are very highly hydrophilic at the surface, there is no problem with the wettability of the separator. This can be seen from the electrolyte uptake and retention curves. All the aluminas retain > 65% of electrolyte after t=100 min. While the polymer separator PP2500 loses about 50% of the absorbed electrolyte at time t=100 min. Therefore, the alumina separators are much better in terms of wettability and retention of the electrolyte, thus leading to improved cell performance.

Table 2.3.3: Calculated porosity of various separators

	Separator	Calculated Porosity (%)
1	PP2500	55*
2	BD1	67 ± 3
3	BD2	56 ± 3
4	BD3	47 ± 3
5	M1	47 ± 3
6	N1	68 ± 3
7	N2	60 ± 3
8	SM1	48 ± 3
9	SM2	47 ± 3
10	SM3	48 ± 3

*Provided by Celgard LLC.

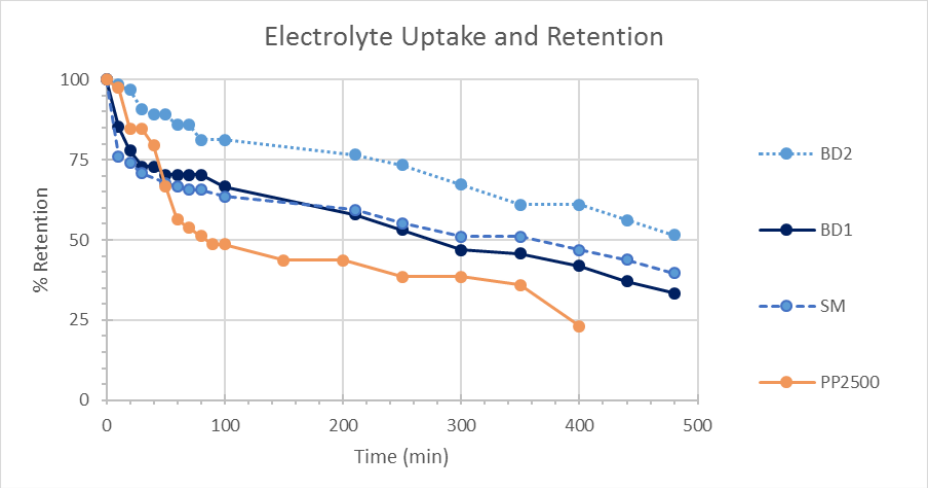

Figure 2.3.8 : Electrolyte uptake and retention of α-alumina separator v/s PP2500

2.3.3 Synthesis and electrochemical analysis of α-alumina separator based cells

Table 2.2.2 contains a list of the α-alumina powders. These powders could be processed well into consistent slurries as well as coated well as a separator on the electrode. LTO is the choice of electrode substrate for two major reasons, first because it is hydrophilic in nature and will assist coating of water based slurry. Secondly because, it is a zero-strain material with low voltage gap between charge-discharge steps when assembled in half cells. [21] Li/LTO cells were assembled from separator samples prepared with aluminas listed in Table 2.2.2 and Table 2.2.3.

Each cell was cycled at 0.2C rate for 100 cycles continuously. To illustrate repeatability and reliability of the results, curves of 3 different assembled cells using the exact same α-alumina powder to prepare separator, are shown in the Figure 2.3.9. Barring some minor experimental errors, the curves almost overlap each other and depict repeatability of data. The various bimodal powders studied in this work, all formed good separators whose cells showed similar, and somewhat identical discharge-charge

characteristics over a total of 100 cycles. The powders being discussed are BD1, BD2, BD3 and SM. The curves can be seen in Figure 2.3.10. The nature of the curves of these half cells, demonstrated stable characteristic curves. The performance curves of these cells is very similar to that of the half cells assembled with Celgard PP2500 polymer type separator.

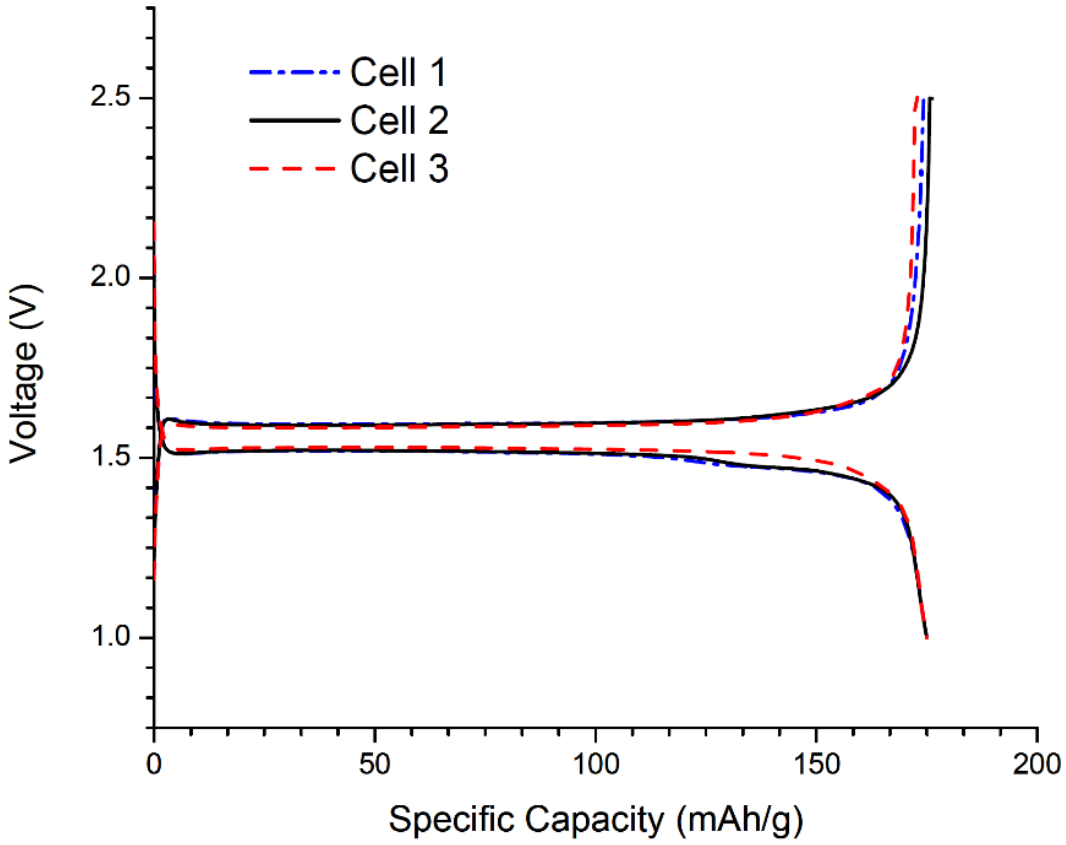

Figure 2.3.9 : Charge-discharge curves of the 25th cycle at 0.2 C cycling rate, of three LTO/Li cells with 45 µm thick coated α-alumina separator; displaying reproducibility.

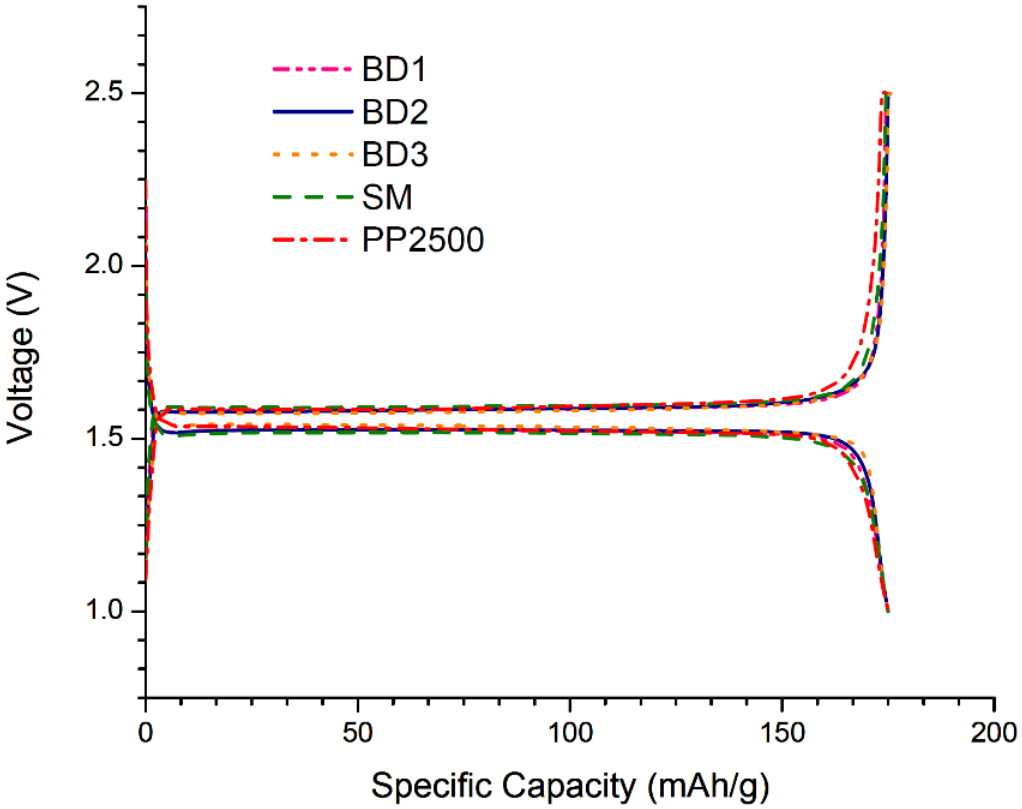

Figure 2.3.10 : Electrochemical performance curves at the 25th cycle of LTO/Li cells with separator composed of mixture of low % of submicron sized and largely micron sized alumina particles. BD1 - 5 % at 0.2 µm and 95 % at 3 µm, BD2 – 50 % at 1 µm and 50 % at 4 µm, BD3 – 2 % at 1 µm and 98 % at 4 µm, SM – 10 % at 0.6 µm and 90 % at 3 µm

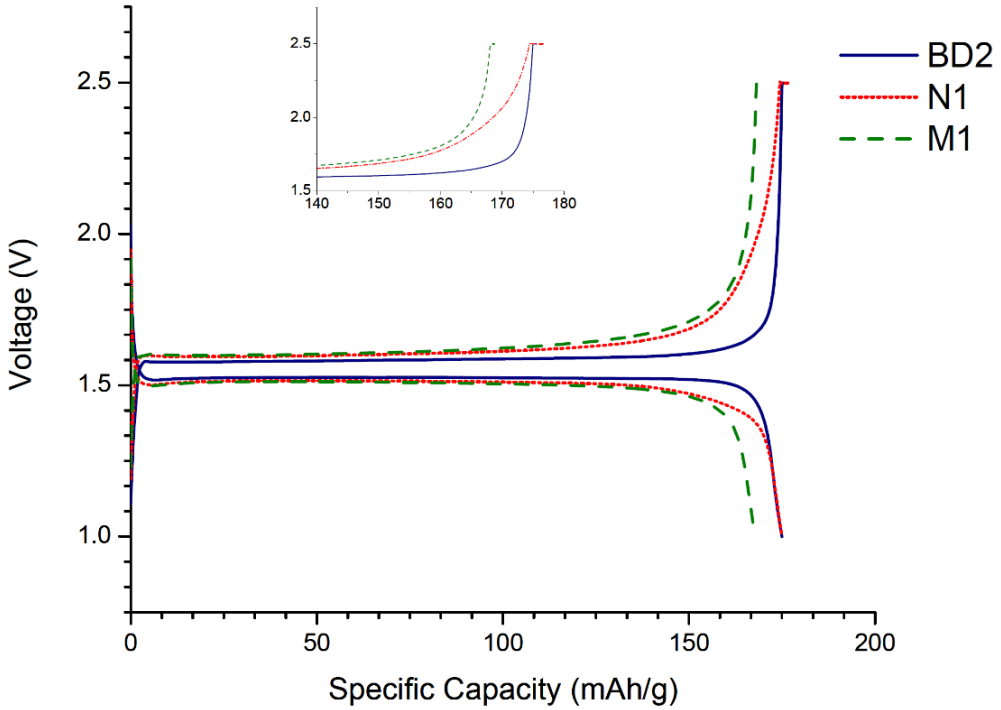

Figure 2.3.11 : Electrochemical performance curves at the 25th cycle of LTO/Li cells with α-alumina composed of varying particle sizes. BD2 – 50 % at 1 µm and 50 % at 4 µm, N1 – 100 % at 0.27 µm, M1 – 100% at 3 µm.

The LTO/Li half cells that were assembled using submicron sized alumina N1 as separator material, displayed a variation from the ideal expected characteristic curve for such a cell. The results can be seen in Figure 2.3.11. The major difference is occurring in the ending region of the voltage-capacity curve of the charging step. This points towards a higher overpotential that may be observed within these particular half cells. The overpotential in this ending region of the charging curve is linked to charge-transfer resistance. This indicates that the LTO electrode performance is clearly affected, within these cells. Since no other component or aspect of cell assembly was altered during the assembly of these cells, this rise in observed overpotential is hypothesized to emanate from the submicron sized α-alumina separator.

No other α-alumina separators exhibited such unstable and varying behavior. Only N1 cells did, and hence indicate the particle interference of alumina with electrode pores as a possible cause. In Figure 2.3.12, SEM images of the LTO electrode at various magnifications were used to try to understand and study the possible effect of the submicron sized particles of alumina N1 on the stable cell performance and electrode integrity of LTO substrate.

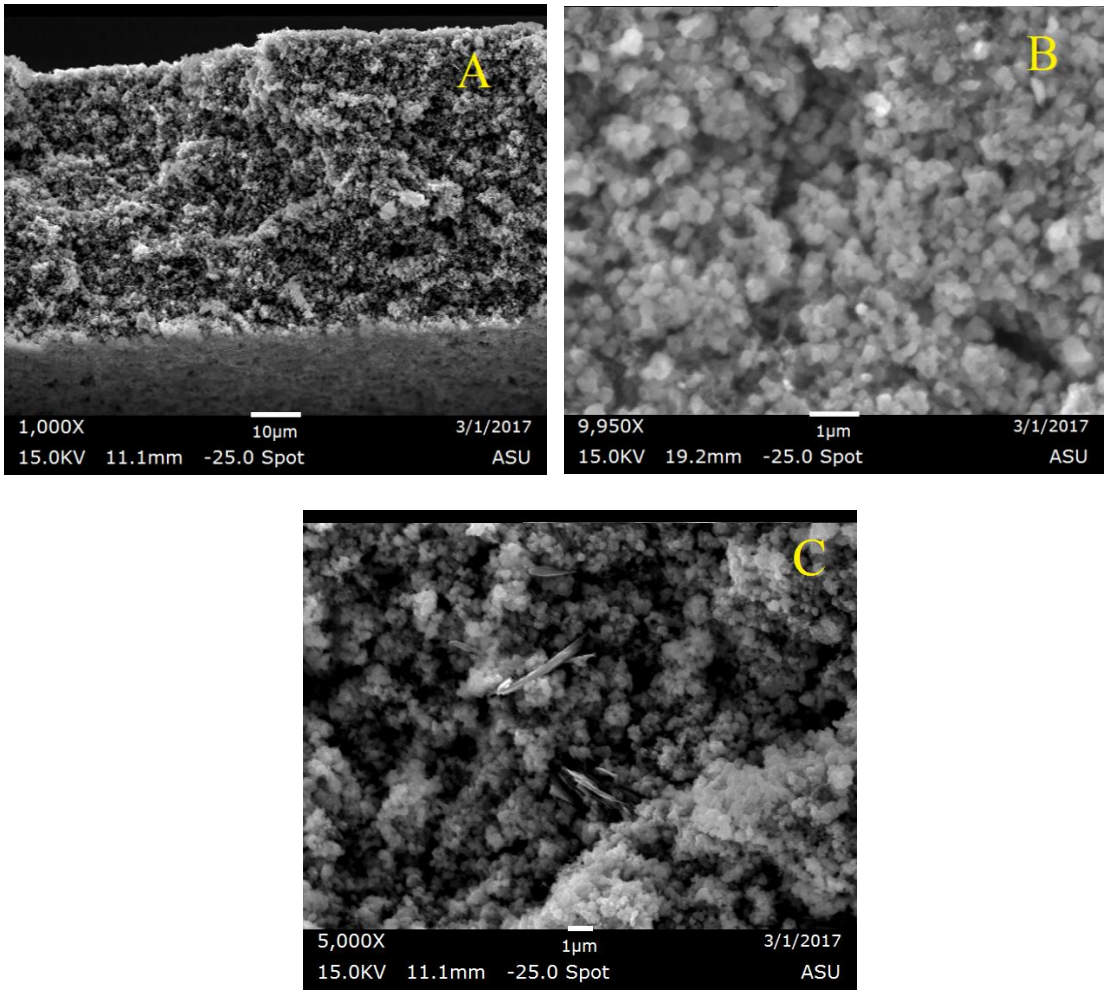

Figure 2.3.12 (clockwise): a] SEM image of the cross-section of LTO electrode substrate and b] SEM images of the surface of the LTO electrode substrate.

A particle size 0.3-0.7 µm with a pore size of about 0.6 µm and lower was observed for the LTO electrode being used as substrate. Hence the submicron sized particles could be affecting cell performance by blocking the pores present on the LTO electrode surface in one way or the other. The BD1 separator that is studied, was composed of > 90% particles with a mean particle size around 3 µm. The remaining particles in BD2 at <10% total volume, are submicron sized. This separator performs almost ideally. Similarly, it is observed that alumina BD2 made up of particles of a bimodal distribution with peaks at 1 µm and 4 µm performs equally well.

This suggests that the presence of submicron sized particles help improve separator coat integrity by ensuring better retention of PVA within the separator layer rather than allowing it to seep into the electrode. It can also be inferred that submicron sized particles will not interfere with the substrate electrode, if they are in a low proportion mixture with mostly micron sized particles. Submicron sized particles in the coated separator should be either avoided or kept to a minimum if a good quality coat is sought and ideal electrochemical performance is desired from the assembled cell. To test this proposition, a two-step approach had to be used. As step one, the separator composed wholly of only unimodal micron sized particles of α-alumina, was prepared and tested in Lithium ion cell assembly as described above. The second step, for confirmation of the results, a mixture with varying amounts of micron to sub-micron sized α-alumina particles was simulated and the resulting separators were analyzed.

To conduct this simulation experiment, two commercially available unimodal α-alumina powders were selected. M1 was selected as a unimodal micron sized powder with a mean particle size of 3 µm. N2 was selected as the unimodal submicron sized

powder with a mean particle size of 0.65 μm. These two powders were physically mixed by weight percent in 3 distinct ratios, to better understand the effect of particle size distribution on Lithium ion cell performance. To easily refer to and describe the varied ratios of micron sized to submicron sized particle alumina powders simulated in this study, the three different ratios selected will be mentioned as SM, SM2 and SM3 respectively. The specific composition of the three mixtures is enlisted within Table 2.2.3 and is provided with a some of their important properties. Just like all other alumina powders studied, these simulated aluminas were cast into separators on LTO electrode as substrate and the tested as per standard procedure. These samples were assembled into Lithium half cells, tested at a 0.2C discharge/charge rate for a total of 100 such cycles.

Figure 2.3.13 represents the formation cycles performed at 0.1 C rate for one cycle only, for each of the simulated powder mixtures. However the actual cell performance can be characterized from the curves in the successive cycles conducted at 0.2 C rate showing uniform curves over 100 cycles. Figure 2.3.14 depicts the resulting electrochemical performance curves for these three types of separators. From the figure, we can conclude that at a concentration of 10% of submicron sized with 90% micron sized particles, the cell gives good performance just as anticipated. But when the ratio of submicron sized particles in the separator exceeds 10% significantly, then the observed cell performance differs a great deal from the anticipated good electrochemical performance that should be seen from the Li ion half cells. As the simulated mixtures were prepared by mixing the powders physically in a weight ratio before slurry preparation, it was important to check for the uniformity of particle size distribution within the coated α-alumina separator layer that was formed. SEM images taken of the

top and cross-section respectively of this fabricated separator layer in Figure 2.3.15, was sufficient to verify the uniformity of the particle distribution.

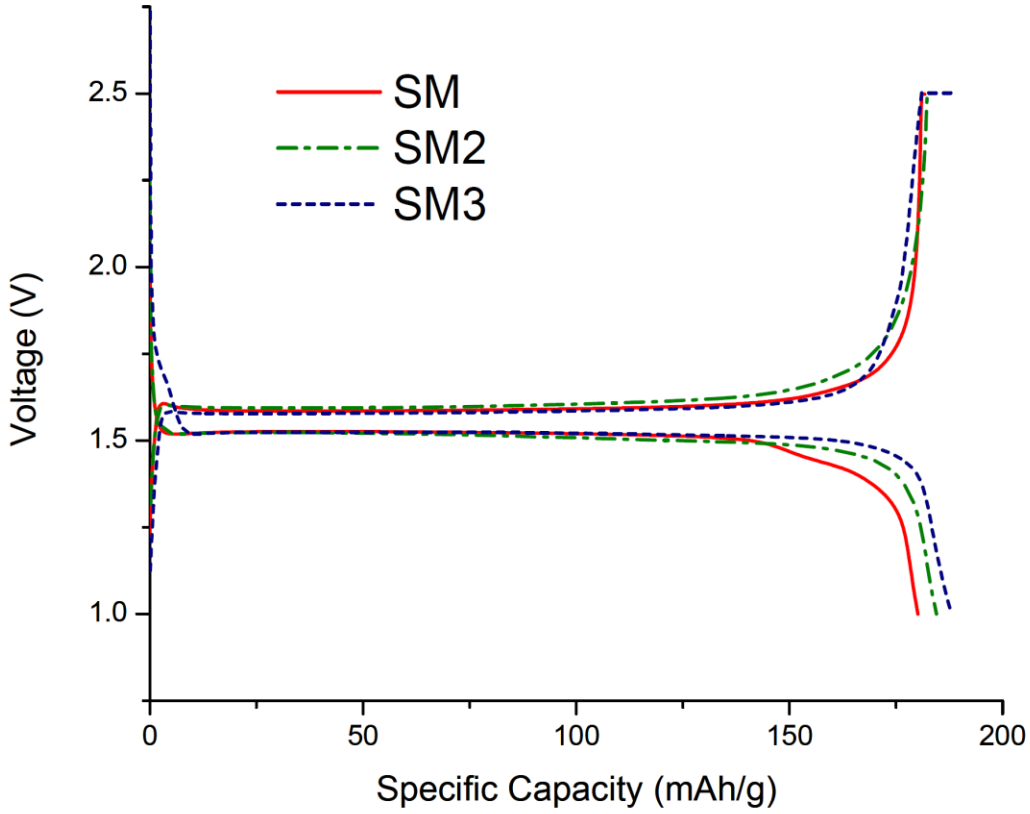

Figure 2.3.13 : Formation cycle discharge charge curves at 0.1C rate of LTO/Li cells with different simulated mixtures of α-alumina as separator.

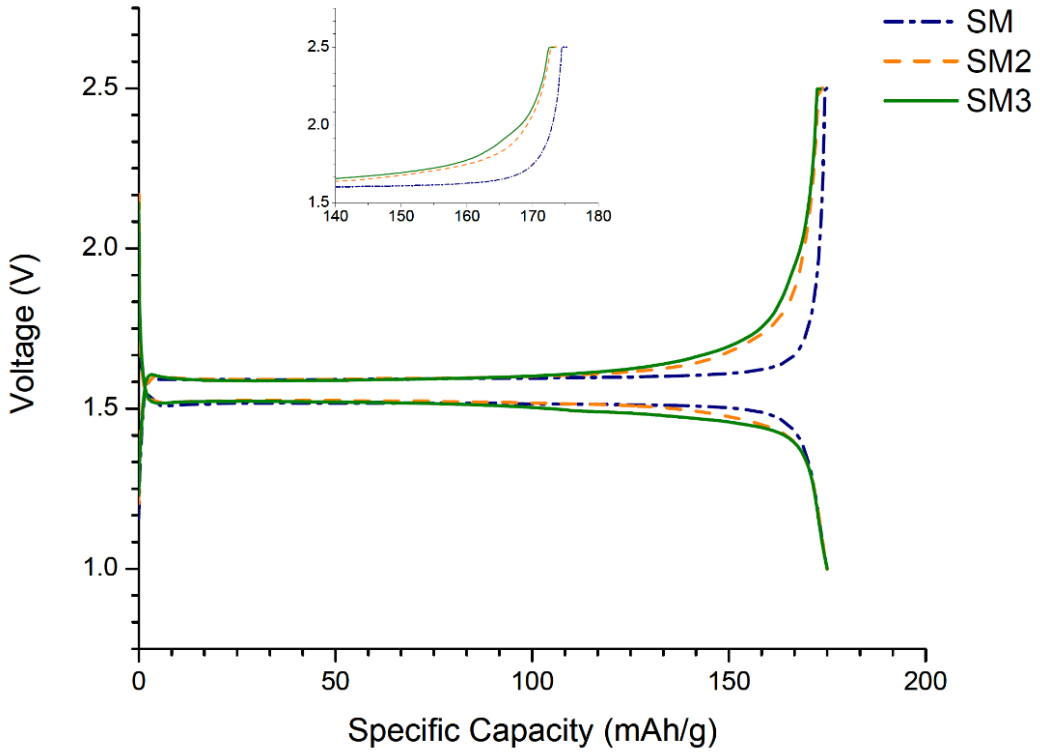

Figure 2.3.14 : Electrochemical performance curves at the 25th cycle of LTO/Li cells with different simulated mixtures of α-alumina as separator.

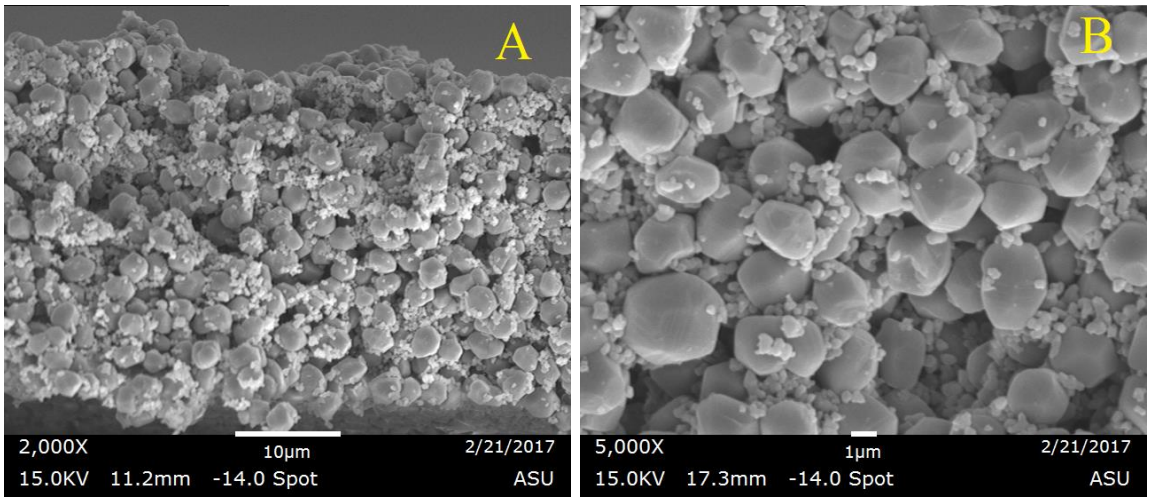

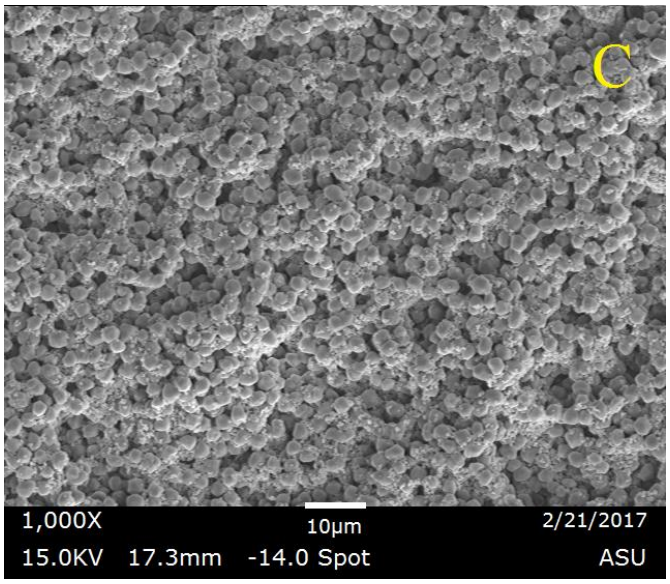

Figure 2.3.15 : (clockwise) a] SEM of cross-section of SM separator (90% M1:10% N2) b] SEM of SM top view at 5k magnification c] SEM of SM top view at 1k magnification.

Separator performance was also characterized using the EIS measurements of the assembled half cells. The curves for the original impedance EIS data are shown in Figure 2.3.16 and Figure 2.3.17. These values were fitted to the simplistic equivalent circuit to obtain fitted curves. Figure 2.3.18 shows accuracy of fitted data vs experimental impedance data. As can be seen there is only marginal error, thus fitted results are reliable. Table 2.3.4 contains impedance data curve-fitted to a simplistic lithium ion model circuit. As mentioned, a basic lithium ion cell equivalent circuit was applied for curve fitting the data obtained from EIS measurements. Figure 2.3.19 shows the equivalent circuit used to fit the impedance data and obtain resistance values for each cell.

The resistance of electrolyte and ohmic resistance due to the separator together contribute to the R1 value in the equivalent circuit. While the physical significance of the R2 resistance value in the equivalent circuit, is linked to the charge transfer resistance at

the interface of the active material. From the results in Table 2.3.4, the impedance data of these cells mainly differs due to separator layer based impedance. [22, 23] The R2 values for the three separators are somewhat similar, while the main difference lies in the R1 values. The thickness of each of these separators was almost the same, excluding a negligible experimental error.

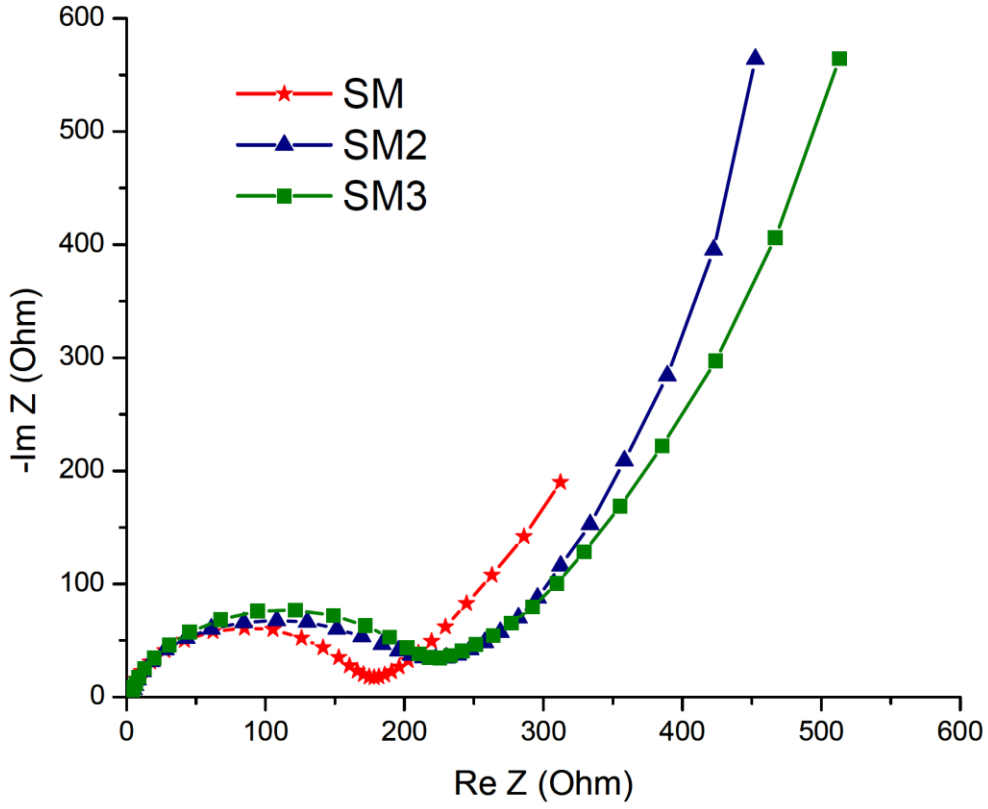

Figure 2.3.16 : EIS experimental data for the three simulated alumina separator based cells at 100% SOC.

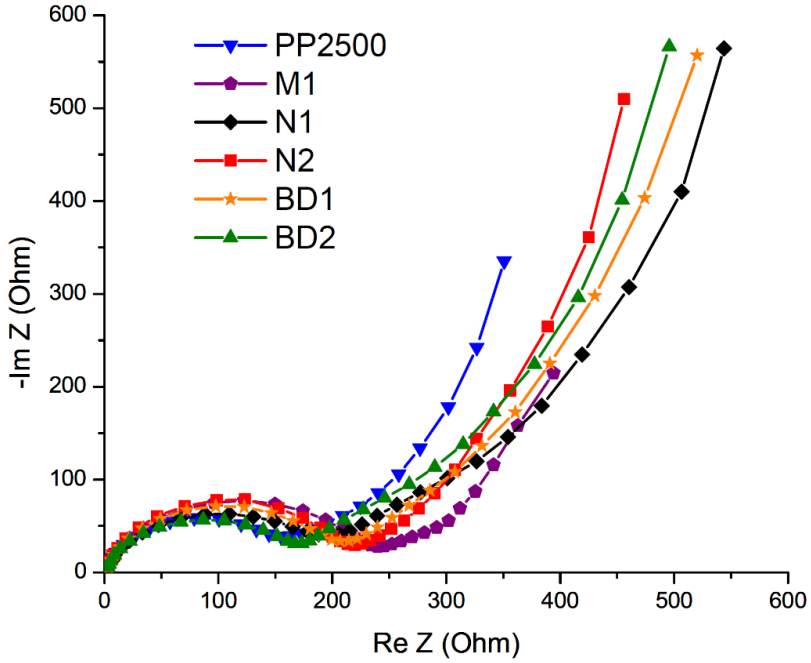

Figure 2.3.17 : EIS experimental data for the various alumina separator based cells at 100% SOC.

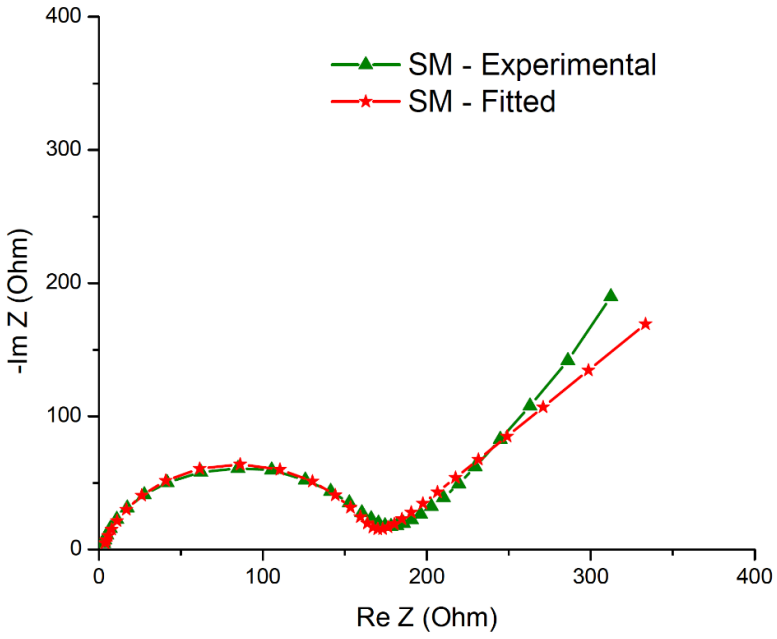

Figure 2.3.18 : EIS experimental data v/s calculated curve fitted data for the same alumina separator based cell at 100% SOC.

Hence, all or any difference in cell impedances can be completely assigned to the effect of the nature of the separator. The three simulated mixtures were prepared from slurries with the same binder composition as % weight of slurry. Any possibility of these variations arising from effects of binder quantity modifications can be ruled out.

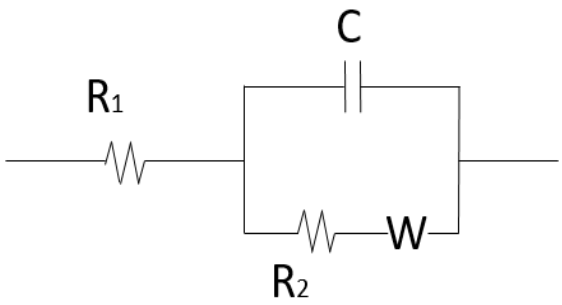

R1 – Resistance of the electrolyte in separator

R2 – Resistance of charge transfer step

Figure 2.3.19 : Equivalent circuit used to fit impedance data

Table 2.3.4: Fitted impedance parameters of LTO/Li cells with various separators

EIS measurements – Equivalent Circuit Curve fitting		
Separator	Resistance (R1) Ω	Resistance (R2) Ω
PP2500	1.7	121.4
BD1	3.96	154
BD2	2.98	148
N1	4.27	149.04
N2	3.48	176.04
M1	4.79	279.97
SM (M1:N2 = 90:10)	3.54	146.94
SM2 (M1:N2 = 80:20)	5.79	165.14
SM3 (M1:N2 = 30:70)	5.2	175

Additionally, the separator formed by SM alumina powder may be more stable owing to the specific type of particle interaction between micron and sub-micron sized particles in the particular ratio that was used. This is supported by the excellent capacity retention of SM cells when compared to capacity retention of SM2 and SM3 cells. As can be seen in Figure 2.3.20, with increasing submicron sized particle content, there is a decrease in retention capabilities of the cells.

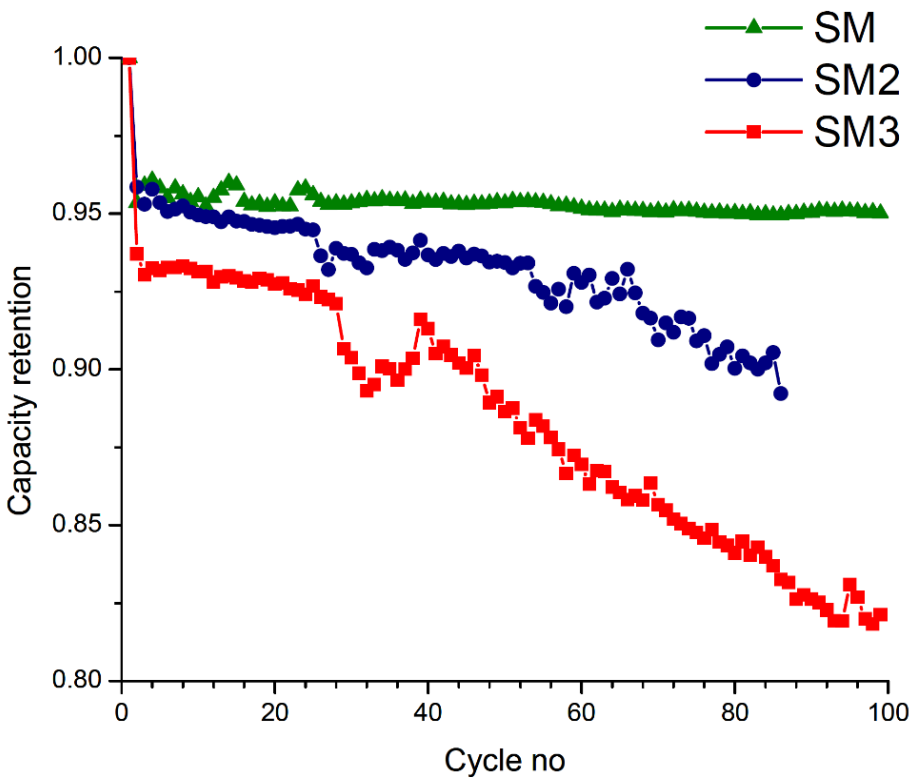

Figure 2.3.20 : Capacity Retention curve for the first 100 discharge cycles of LTO/Li cells with different simulated mixtures of α-alumina as separator

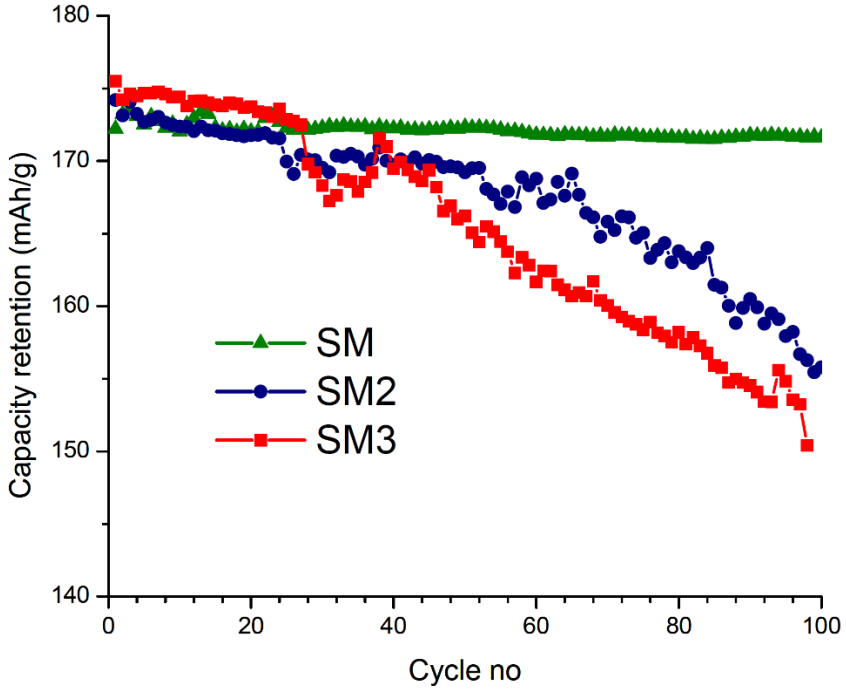

Figure 2.3.21 : Discharge Capacity Retention curve for 100 cycles at 0.2C discharge rate of LTO/Li cells with different simulated mixtures of α-alumina as separator

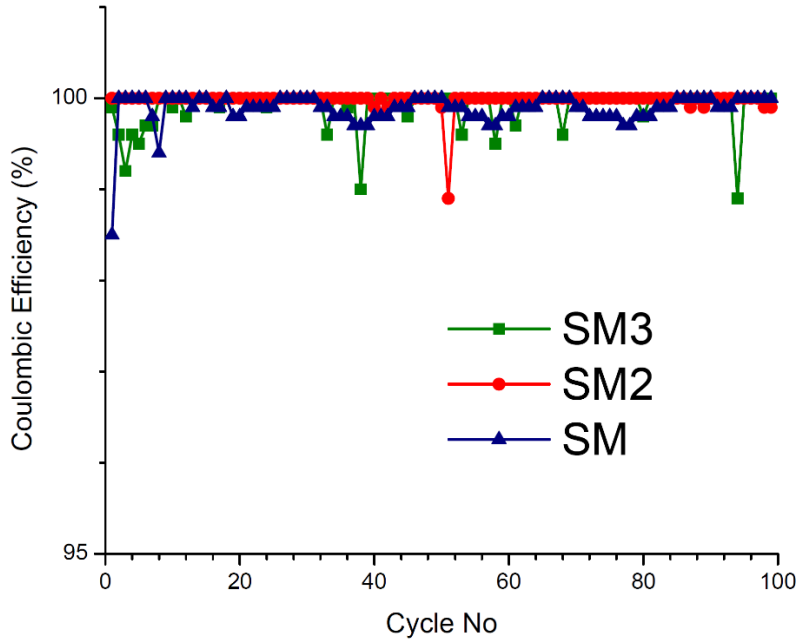

Figure 2.3.22 : Coulombic Efficiency for the 100 cycles at 0.2C discharge rate of LTO/Li cells with different simulated mixtures of α-alumina as separator

As mentioned earlier, using only micron sized particles for the fabrication of the α-alumina separator was an approach that was tried. In that case, assuming the only consideration to achieving good separator fabrication and resulting good cell performance was avoiding the use of submicron sized particles. Then for the micron sized α-alumina M1, a high quality separator should form with equally good half cell performance. But, this was not supported by the results. Instead, evidently from Figure 2.3.11, M1 separator based cells exhibit a major resistance at the far end of the charging curve.

From the processing of the slurry, it is clear that, M1 powder particles are very cohesive. The reason for the exact nature of performance observed in M1 cells can be associated with the possible seepage of the PVA binder solution between the inter-particle spaces of alumina M1 when the slurry is being coated. This idea is backed up by the observation of poor binding of the M1 separator layer to the substrate electrode as seen in Figure 2.3.8.

2.3.4 Effect of excess binder percolating to electrode substrate on Li ion cell performance

It is clear that M1 separator binds poorly to the substrate electrode which leads to the subsequent poor performance observed in assembled half cells. To identify the cause behind this observed behavior, a study was conducted as follows. In the ratio 0.7 : 1.1 by weight respectively, a dilute solution consisting of 5 wt % PVA binder was added to water. This exact ratio of components was selected so as to effectively compare the achieved results with that of the M1 separator half cells. The results of M1 separator have been described in detail, in the work above.

The dilute solution of PVA was then coated directly by the two-step blade coating process on top of LTO electrode and the samples were processed in the exact same way as the α-alumina coated LTO electrode samples. LTO electrode samples coated with dilute PVA solution were assembled into Li/LTO half cells and used Celgard PP2500 as separator material. The cells were cycled by the standard procedure at 0.2C rate for all 100 cycles. The resulting electrochemical performance curves of these cells is shown in Figure 2.3.23.

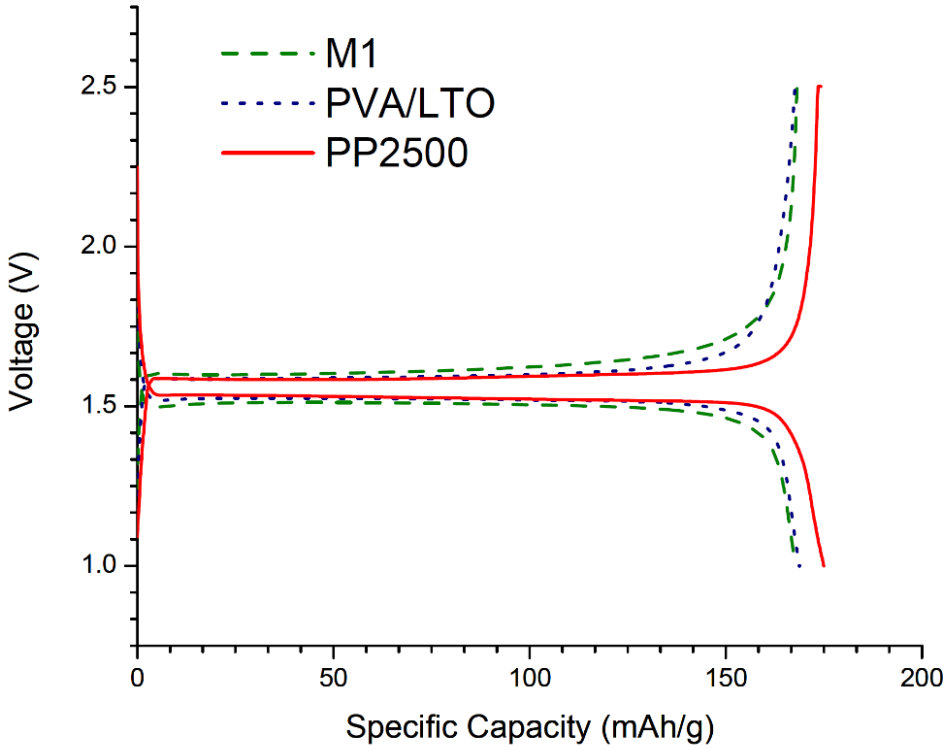

Figure 2.3.23 : Electrochemical performance curves of LTO/Li cells with M1 unimodal micron sized α-alumina (3 µm) as separator v/s cells with PP2500 as separator but LTO electrode coated with PVA and ordinary cells with PP2500 as separator.

The curves of PVA coated electrode half cells are plotted versus ordinary PP2500 separator half cells and M1 separator containing half cells, to get a good comparison.

Clearly in Figure 2.3.23, the nature of the M1 charging curves is very similar, to that of the PVA coated electrode half cells. There is a similar drop in achieved capacity as well, which would justify that PVA solution is affecting electrode performance in both these cells in the same manner. Thus confirming that PVA binder loosely bonded to the surface of the LTO electrode significantly affects cell performance.

As reported by Linghui et al. [24] for ceramic coated polymeric separators, increasing the content of PVA binder negatively affects the electrolyte wettability of alumina coated polymeric separator layer. Lin and co-workers [14] reported, an increased resistance in the charge transfer step was observed with modifications to the slurry PVA content. This establishes that PVA likely percolates into LTO electrode surface during the fabrication step of M1 separator.

The Nyquist plots for the three LTO/Li cells reported in the work above can be viewed in Figure 2.3.24. EIS data of each of these half cells was fitted to a basic version of Li-ion cell equivalent circuit using EC-Lab software. The impedance values were obtained and listed in Table 2.3.2 along with standard deviations. The Nyquist plot of -ImZ v/s ReZ for a Li-ion cell, can be categorized qualitatively into 3 significant parts. The intercept on the x-axis indicates separator contribution towards internal resistance and is generally a direct function of separator thickness. The second part of the curve, the semicircular region indicates contributions of separator and SEI layer impedance.

The linear part of the curve which is third and final part of this curve, represents electrode charge-transfer step impedance or electrode associated impedance. [14] Hence, if we observe Figure 2.3.24 carefully, we can conclude on a purely qualitative basis that, percolated PVA binder on electrode surface does affect the electrode performance to

some extent. So, a similarity in the linear part of the Nyquist plot is observed due to this reason for PVA coated LTO/Li half cells as well as the M1 separator coated LTO/Li half cells.

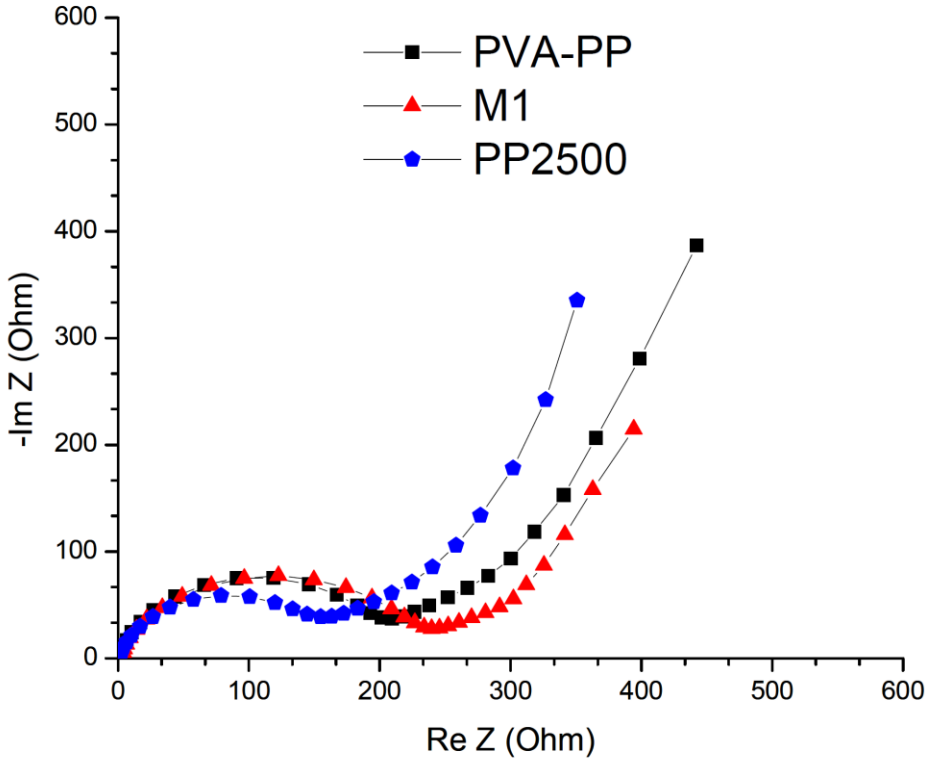

Figure 2.3.24 : Nyquist plots for PVA coated LTO cells with PP2500 separators v/s cells with M1 separator v/s cells with PP2500 separator.

Lastly FTIR analysis of various coated LTO samples was conducted, in order to confirm or reject this hypothesis. First the separator coated LTO samples had to be gently brushed to remove the coated α-alumina layer as a way of sample preparation for this experiment. Then the LTO samples thus obtained, were used in the FTIR analysis. A total of 6 types of samples were tested with FTIR. Plain pristine LTO electrode sample, LTO coated with PVA binder solution, LTO which had been coated with M1, BD2 and N2

respectively, and lastly PVA salt were all analyzed to provide a comprehensive study in the analysis.

In Figure 2.3.25, only the samples of M1, and PVA coated LTO, exhibit transmittance peaks at 3300 cm^{-1}, 2950 cm^{-1}, 1740 cm^{-1}, 1560 cm^{-1} and 1150 cm^{-1}. The two peaks of 2950 cm^{-1} and 1740 cm^{-1} correspond to peaks observed for PVA, with 2840-3000 cm^{-1} representing C-H bonds from alkyl group and 1740 cm^{-1} representing the C=O bonds. The stretching observed at 3300 cm^{-1} is attributed to presence of OH bonds from the alcohol. The peaks at 1560 cm^{-1} and 1150 cm^{-1} result due to the presence of CH_2 and C-O bonds respectively. [25, 26] Therefore, it would indicate and confirm percolation of PVA into the substrate electrode for these two specific samples.

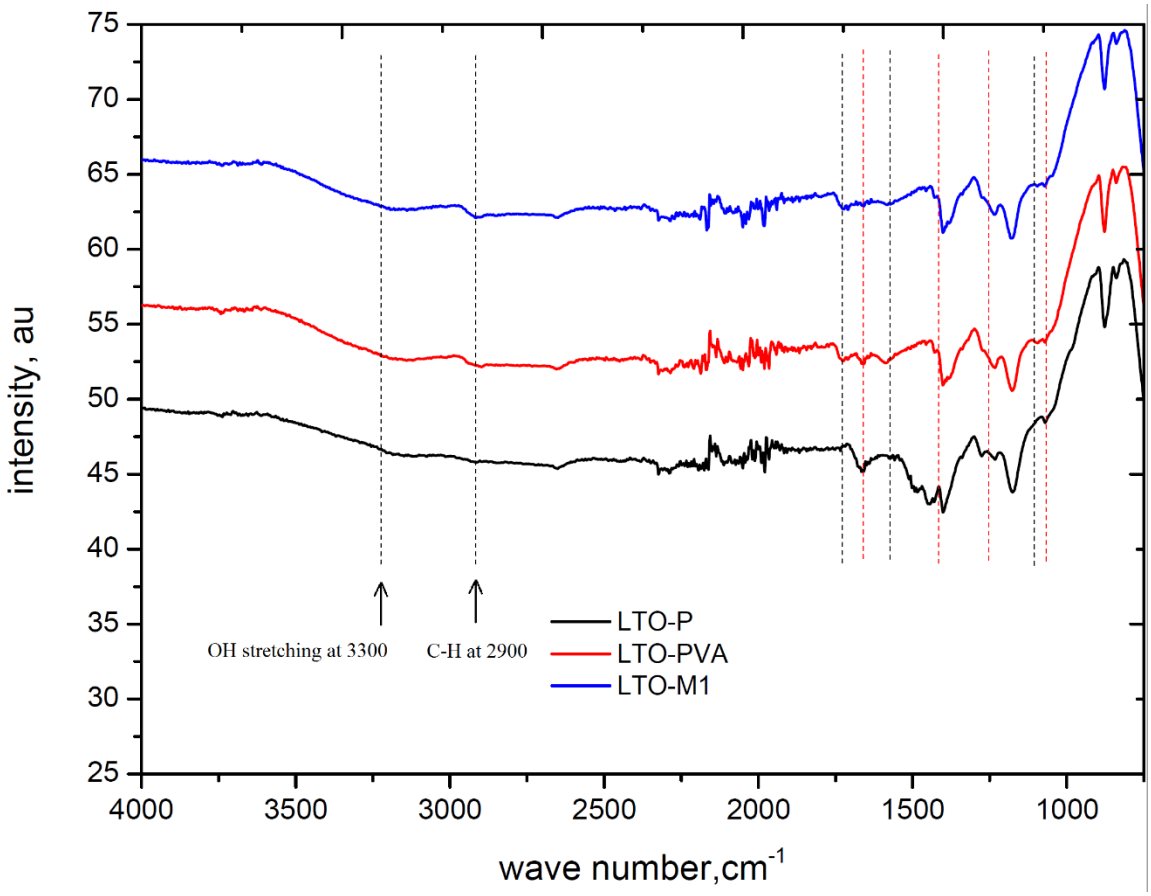

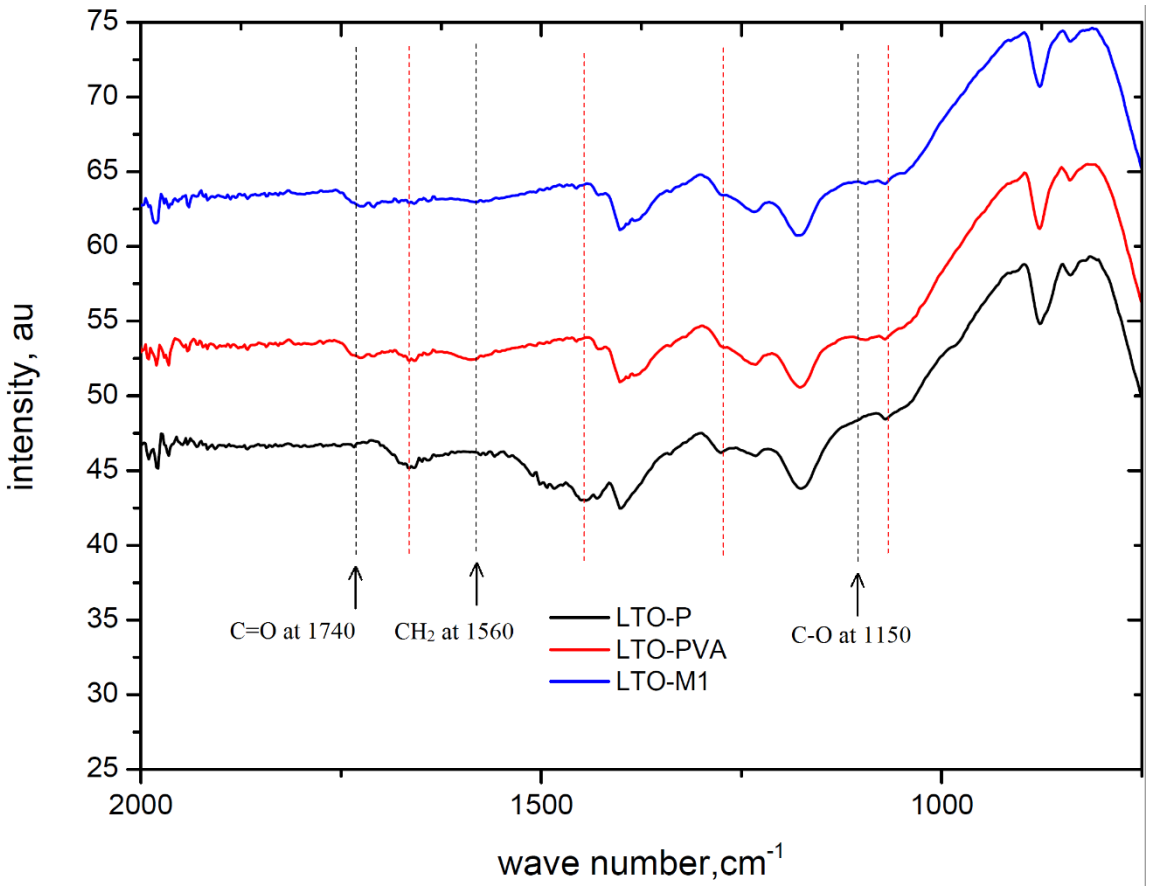

Figure 2.3.25 : FTIR curves for M1 α-Alumina separator coated and stripped electrodes v/s plain LTO electrode v/s PVA solution coated LTO electrode

In Figure 2.3.26, the samples of BD2, N2 and SM3 coated and stripped LTO electrode do not show the characteristic peaks seen of bonds observed for PVA samples. Thus, confirming the hypothesis regarding seepage of PVA into LTO electrode in case of M1 sample.

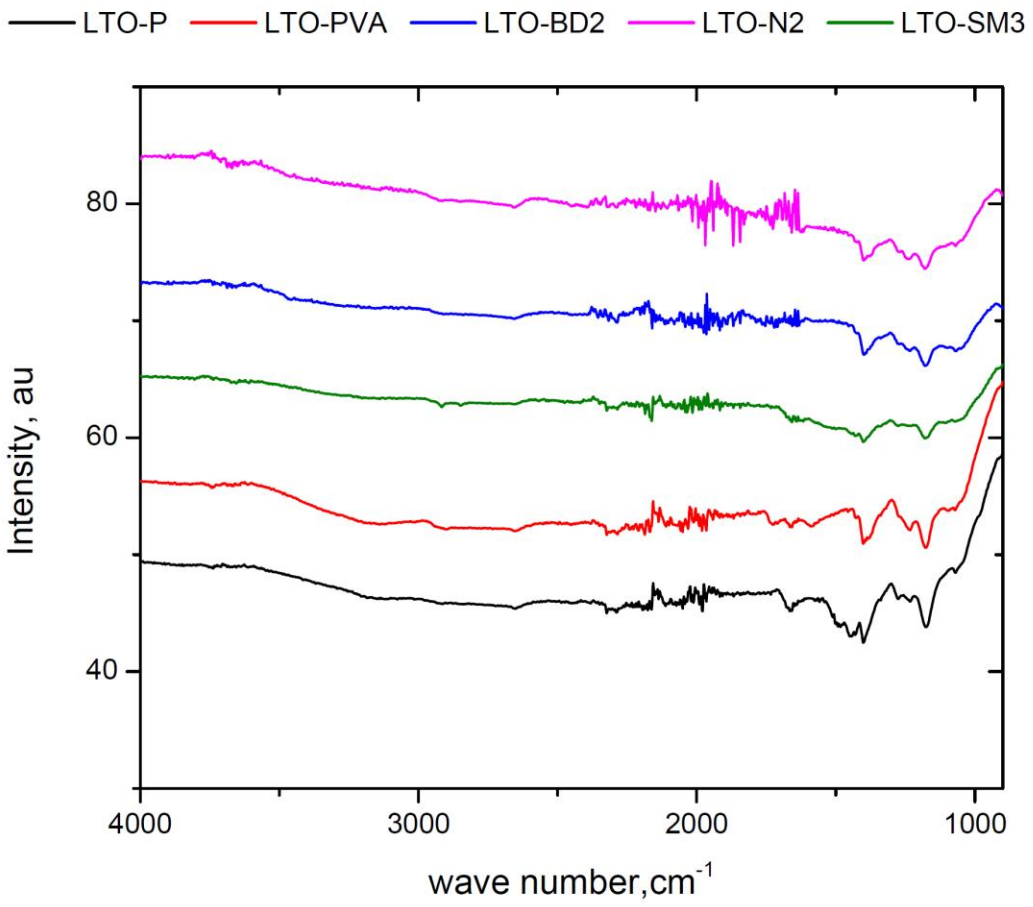

Figure 2.3.26 : FTIR curve for other α-Alumina separator coated and stripped LTO electrode samples v/s plain LTO electrode v/s PVA solution coated LTO electrode.

2.4 Summary

The results in this study can be summarized under a few distinct categories. The results from fabrication step point to poor processability of larger particle size aluminas for obtaining separators by the method studied in this work. Very large size particles failed to constitute into a slurry of the required consistency. Large size particles despite forming into a homogenous slurry were unsuccessfully in forming a separator coating on the electrode.

Alumina with particles of size 7 µm and below were successful in formation of slurries and fabrication of separators. Unimodal micron sized particles of alumina showed ability to form visibly continuous separators on the electrode. But the stability of such separator coating was poor. The non-unimodal or bi-modal micron sized particle aluminas prepared continuous separators with strong adherence properties.

Cell performance of cells containing such alumina separators varied significantly depending on particle size. For submicron sized alumina particles, of size less than that of the substrate electrode particles, poor and inconsistent cell performance was observed. While for alumina particles with size greater than or equal to 1 µm, good and consistent performance was observed. Also, the unimodal particles which lead to mechanically weak separator, also displayed poor cell performance.

Finally leading this study shines light on alumina with particle size greater than substrate electrode particles and lower than 7 µm with a bimodality in distribution as the most successful or useful type of alumina powders for this application. Confirmatory results to support the same were obtained through the simulation powder section discussed above.

CHAPTER 3

CONCLUSIONS AND RECOMMENDATIONS FOR FUTURE WORK

3.1 Conclusion

This work offers significant conclusive evidence and analysis regarding the requirements to be considered for obtaining high quality, stable α-alumina separators. To be able to scale up the process to an industrial level, it is required that the raw materials or precursors for a process are easily available and can be sourced. This includes proper identification of properties and parameters that would lead to repeatable production. While previous work on electrode supported α-alumina separators has proven the ability of easy scale up for this process, the governing parameters were not discussed.

In this work, it is found that, electrode supported α-alumina separator may be formed well dependent whether two important considerations are satisfied or not. The separator two-step blade coating process is enabled by a homogenous and consistent slurry formation. It is inferred from the results, that a certain specific type of distribution of α-alumina particles is required to obtain a good quality slurry. Thus, by seeking the desired distribution in particle size, a high quality non-interfering coating of the separator can be successfully formed on the electrode. The desired particle size distribution can be categorized as per the observed results which are confirmed through thorough analysis.

Particle size of α-alumina powder restricted to under 10 μm is advised if the blade coating process is to be utilized for coating a separator as thin as 40 μm or lesser. Selection of this parameter results in a continuous and unvaried coat of the separator. Slurry quality specifically for the two-step blade coating method for α-alumina, was optimized with a bimodal distribution of its particles. The bimodal distribution peaks

were identified to be approximately at around 1 µm or under and at 3 µm respectively. Preferred slurry viscosity is attained by using such a distribution and assists in the formation of high quality separator layer.

While slurry consistency and quality requirements were met by involving particles under 1 µm, from the perspective of cell performance, it was observed that submicron sized α-alumina particles with mean particle size similar and specifically lesser than that of the electrode material led to a poor outcome. The reason being that, submicron sized α-alumina particles possibly were interfering with the electrode pores and affecting its performance. With good reliable cell performance as the focus, the α-alumina particles in the separator layer must be restricted to a minimum.

Another critical conclusion that can be drawn from this study is that, a unimodal distribution of micron sized particles cannot be used to form these separators. Specifically, we can attribute the percolation of binder material from such a slurry, into electrode substrate as the cause leading to poor observed cell performance. To conclude a bimodal particle size distribution is sought for this application. The percentage of submicron sized particles must be limited to < 10% by weight. The remaining separator material shall be formed of micron sized particles. This optimized ratio led to the formation of a sturdy, inactive separator. The cells assembled with separator consisting of the optimized ratio were comparable to a commercial polymeric separator cell. Therefore, this optimized composition of particle size distribution forms a good quality slurry, as well as a high quality α-alumina separator and gives good cell performance. Thus, complying with each step involved in the study.

3.2 Recommendations

1. From the experiments conducted and described in this thesis and considering the results and outcomes, the following recommendations are suggested for future work.
2. The performance of these separators should be tested in the pouch cell assembly. Pouch cell assembly requires a significantly higher dimensional stability from cell components when compared to a coin cell. Furthermore, the total area of uniform separator coating required will be much higher, thus serving as a true test to quantifying the ability of these separators to be scaled up to industrial scale.
3. The mechanical integrity of the various grades of alumina formed separators should ideally be recorded by designing an appropriate experiment for the same. As seen in this study, some alumina powders despite forming a uniform and consistent separator, the formed separator tends to be brittle and cakes off easily. So, a study of this nature will be useful. This can be approached in two ways. It can be conducted via direct mechanical testing of separator samples. It can also be investigated through observed electrical performance of pouch cells with these separators but when subjected to different external constraints such as folding or bending.
4. Although a qualitative understanding of alumina slurry viscosity was achieved in this work, it is advisable to numerically quantify the slurry viscosity. This can provide more useful when investigating other ceramic powders using the same blade coating method. It could also shed light on inter-particle behavior in slurry v/s when in powder form.

5. Similarly, an accurate quantitative measurement of blade coating speeds should be conducted. This will assist a broader study of multiple ceramic materials as separator.
6. The effects of particle size and distribution are observed, analyzed and confirmed α-alumina. It would be interesting to compare the results of α-alumina particle interactions and see if they hold for other ceramic materials just the same. Or there may be different findings for each ceramic material possibly related to surface characteristics. This avenue should be pursued to successfully seek more types of electrode coated ceramic separators.

REFERENCES

[1] H. A. Kiehne, Battery Technology Handbook, Second Edition, (2001), 405-406.

[2] J. B. Goodenough, K. Park, J. Am. Chem. Soc. 2013, 135, 1167−1176.

[3] W. Shin, D. Kim, J. of Power Sources 226 (2013) 54-60.

[4] J. Choi, S. H. Kim, D. Kim, J. of Power Sources, 195, (2010), 6192–6196.

[5] Y. Zhang, Z. Wang, H. Xiang, P. Shi, H. Wang, J. of Membrane Science 509 (2016) 19–26.

[6] X. Huang, J. Solid State Electrochem (2011) 15:649–662.

[7] S. S. Zhang, K. Xu, T.R. Jow, J. of Power Sources 140 (2005) 361–364.

[8] S. S. Zhang, J. of Power Sources 164 (2007) 351–364.

[9] H. F. Xiang, J. J. Chen, Z. Li, H. Wang, J. of Power Sources 196 (2011) 8651– 8655.

[10] J. Chen, S. Wang, L. Ding, Y. Jiang and H. Wang, J. Membr. Sci., 461, 22–27 (2014)

[11] M. He, X. Zhang, K. Jiang, J. Wang and Y. Wang, ACS Appl. Mater. Interf., 7, 738-742 (2015).

[12] M. Kim, Y. Nho, J. H. Park, J Solid State Electrochem (2010) 14:769–773.

[13] K. Hamano, US Patent 5981107 A, Nov 9, (1999).

[14] W. Mi, G. Sharma, X. Dong, Yi Jin, Y.S. Lin, J. of Power Sources, 305, (2016) 209-216.

[15] G. Sharma (2016), Improved Synthesis and Thermal Stability of Electrode-supported α-alumina Separator for Lithium Ion Batteries, M. S. Thesis, ASU.

[16] Q. Wang, P. Ping, X. Zhao, G. Chu, J. Sun, C. Chen, J. of Power Sources, 208, (2012), 210–224.

[17] S. Tobishima, J. Yamaki, J. of Power Sources, 81–82, (1999), 882–886.

[18] K. G. Harrya, A. Johnson, J. of Archaeological Science 31 (2004) 1567-1575.

[19] Xueliang Dong, Wanliang Mi, Linghui Yu, Yi Jin, Y.S. Lin Microporous and Mesoporous Materials 226 (2016) 406-414.

[20] E. Pohjalainen, S. Räsänen, M. Jokinen, K. Yliniemi, D. A. Worsley, J. Kuusivaara, J. Juurikivi, R. Ekqvistf, T. Kallio, M. Karppinen, J. of Power Sources, 226, (2013) 134-139.

[21] E. Pohjalainen, T. Rauhala, M. Valkeapa, J. Kallioinen, and T. Kallio, J. Phys. Chem. C 2015, 119, 2277−2283.

[22] D. Andrea, M. Meilera, K. Steinera, H. Walza, T. Soczka-Gutha, D.U. Sauer, J. of Power Sources 196 (2011) 5334–5341.

[23] D. Andrea, M. Meilera, K. Steinera, H. Walza, T. Soczka-Gutha, D.U. Sauer, J. of Power Sources 196 (2011) 5349–5356.

[24] L. Yu, Y. Jin, Y. S. Lin, RSC Adv., 2016, 6, 40002–40009.

[25] H. S. Mansur, C. M. Sadahira, A. N. Souza, A. P. Mansur, Materials Science and Engineering C 28 (2008) 539–548.

[26] R. A. Nyquist, Interpreting Infrared, Raman, and Nuclear Magnetic Resonance Spectra.

APPENDIX A

USING IMAGEJ AND MATLAB TO CALCULATE PARTICLE SIZE DISTRIBUTION OF α-ALUMINA SEPARATOR

The particle size distribution data was obtained by analyzing multiple SEM images of the surfaces of the coated α-alumina separator layer. The SEM images were analyzed to measure all visible particles in terms of particle diameter. The particle diameter measurements were conducted with the aid of the ImageJ Software made available by the NIH. It was used to determine the particle diameter using the straight length measurement tool.

The procedure begins by opening the SEM image of the desired α-alumina separator. Next, select the Straight length measurement tool or the line shape in the toolbar, and use it to measure the scale present on the SEM image by spanning the line over the scale bar. Then, Select Analyze, and Set Scale. In the window that pops-up, enter Known Distance as the scale value of the SEM image. Enter units as microns. Next, Select Straight length measurement tool and use the tool to measure the diagonal length/diameter of a single particle. Next, Select Analyze and Measure. The reading for length will be measured into a data file in terms of pixels and microns. Continue to repeat this procedure to measure all completely visible particles in the given SEM image. Save the data file once all the particles measurements have been recorded.

Process the data using a data analysis software. Divide the particle size range into smaller sub ranges and calculate the total number of particles under each sub range. Compute mean particle size for each sub range. Prepare and plot the data for cumulative no of particles v/s mean particle size. Using MATLAB software, apply the curve fitting tool to get a good fit to the data. Use the resulting equation function obtained from the curve fitting, and differentiate it in the MATLAB software. Compute data for

differentiated no of particles v/s mean particle diameter. The resulting curve obtained approximately represents the particle size distribution of the powder on a no of particles basis.

Calculate the approximate mean particle volume corresponding to the mean particle size values. Multiply number of particles in each sub range with the corresponding mean particle volume. Prepare and plot the data for cumulative volume % v/s mean particle size. Using MATLAB software, apply the curve fitting tool to get a good fit to the data. Use the resulting equation function obtained from the curve fitting, and differentiate it in the MATLAB software. Compute data for differentiated volume % v/s mean particle diameter. The resulting curve obtained approximately represents the particle size distribution of the powder on a % volume basis.

APPENDIX B

GLOVEBOX OPERATION

B1. Glovebox Operation

1. Begin by refilling the small antechamber using UHP Argon gas to diffuse the vacuum. Thus, permitting the door of the antechamber to be opened.
2. All samples should be loaded within petri dishes and placed within the small antechamber, with an inert object placed on the covers to prevent sample disruption during proceeding purge cycles.
3. Switch the vacuum pump on. Then proceed to purge the antechamber thrice. This is done by successively evacuating and refilling, the antechamber with working gas for a total of three times.
4. Next, after wearing nitrile gloves, insert hands into the glovebox gloves and wear a pair of nitrile gloves over those as well.
5. Proceed to open antechamber from within the glovebox and access the samples.
6. Follow standard procedure to assemble a cell. Once the cell is assembled, return all samples and cells to the small antechamber and close the door securely from the inside.
7. Take care to remove the nitrile gloves worn within the glovebox before carefully disengaging from the gloves of the glovebox. Then proceed to collect the cells and samples from the external door of the small antechamber.
8. Securely fasten the outer door of the antechamber. Then switch on the vacuum pump to place the antechamber on vacuum, safely sealing it.

B2. Glovebox Catalyst Regeneration

1. When the catalyst column in the glovebox cannot maintain O_2 and H_2O content under 0.5 ppm, the catalyst bed needs to be regenerated.
2. Click on the “Regen” switch on the control panel located on the front side of the glovebox system.
3. Upon completing step 2, the glovebox panel display will show “Column Valves Open”. At this point, using the toggle switch, these valves must be closed to seal the glovebox from the catalyst column.
4. Next, the display will prompt to check for regeneration gas flow and will display “Is REGEN flow OK?”.
5. The system will automatically open the required valves.
6. Ensure flow of regeneration gas from the gas cylinder is maintained at 20 mm. The manual flow meter, located next to the inlet for regeneration gas can be used to observe and confirm adjustments to flow rate.
7. Once desired flowrate has been set, use the toggle switch on the control panel to select “Yes”.
8. If step 7 is conducted without adjusting regeneration gas flow to required amount, the operation will be canceled.
9. If all the steps from 1-9 are correctly followed, the glovebox will begin the process for regeneration of catalyst. During the process of regeneration, the control panel will display time left and stage of regeneration being conducted for the user’s reference.

APPENDIX C

PROCEDURE TO ASSEMBLE HALF-CELLS

1. Select negative case from the CR2032 coin cell casing.

2. Position the LTO electrode or alumina coated LTO electrode which has been cut to a disk of 16 mm diameter, and place it in the negative case. In case of bare LTO electrode, place polymeric separator over LTO electrode during assembly.

3. Add 120-156 μL of $LiPF_6$ electrolyte on the separator.

4. Place a flattened chip of Lithium foil having a diameter of 15.5 mm on top of the separator layer.

5. Over the Lithium chip, place 2 spacers of same dimensions.

6. Then place one spring atop the two spacers.

7. Place the positive case from the CR2032 coin cell casing over the assembled cell components.

8. Position the cell within the crimp stage of the crimping machine (MSK-110, MTI) and apply a pressure of 300-500 psig.

9. Wipe down the cell exterior to rid it off any excess electrolyte released during crimping.

APPENDIX D

HALF CELL CYCLIC TESTING

1. Load the cell onto a port on the NEWARE BTS3000 battery tester. Position the cell in the alligator clip jaws securely. The side of the coin cell that contains anodic material is attached onto negative (black) wire, while the side of the coin cell containing cathodic material is attached to the positive (red) wire.

2. On the NEWARE software, select the icon representing a single cell test channel. Right click on the channel and choose the ‘Startup’ option.

3. The cycling steps can be selected as per the order mentioned below,

(a) Rest cell for 24 hours.

(b) Rest cell for 60 seconds.

(c) Constant Current Discharge of cell at 0.1 C rate.

(d) Rest cell for 60 seconds.

(e) Constant Current Constant Voltage (CCCV) Charge of cell at 0.1 C rate. An ‘End Current’ of 15% * charging current is set for this step.

(f) Rest cell for 60 seconds.

(g) Cycle the cell at 0.1 C rate for two cycles. This serves as the formation cycles of the cell.

(h) Rest cell for 60 seconds.

(i) Constant Current Discharge at the C rate established in the literature or as required.

(j) Rest cell for 60 seconds.

(k) Constant Current Constant Voltage (CCCV) Charge at desired C rate. Set An ‘End Current’ of 15% * charging current is set for this step.

(l) Rest cell for 60 seconds.

(m) Allow the cell to continue cycling by itself, for a number of cycles as pre-determined and desired.

(n) Upon completion of cycling choose ‘End’.

4. Upon completion of cell cycling, the cell should be removed from the jaws of the alligator clips.

APPENDIX E

ELECTROCHEMICAL IMPEDANCE SPECTROSCOPY

1. PARSTAT 2263 EIS station used has a total of four terminals. They are as follows - Sense, Working-electrode, Counter-electrode and Reference. Connect the sense and working-electrode to positive end of the jaws of the alligator clip and connect Counter-electrode and Reference to the negative end of the jaws of the alligator clip.
2. Place the cell into the jaws of the alligator clip after it has been rested for a period of 24 hours. The side of the coin cell containing cathodic material should face positive end and the side with anodic material should face negative end of the alligator clip.
3. Open the PowerSuite software, select Tools > Database Management > Create New Database > Create a .mdb file.
4. Then, select Experiment > New > Browse > Select database file created from Step
5. Go to PowerSine > Single Sine > Select Default SS.
6. Under Scan Definition, select start frequency of 100 KHz, select end frequency of 10 mHz.
7. Select points/decade as 5.
8. Click on logarithmic point spacing with AC amplitude set at 10 mV rms and select DC potential as 0 V.
9. Select finish, to run the test and acquire the Nyquist plot and impedance data for the cell.

APPENDIX F

POROSITY MEASUREMENT OF ALUMINA SEPARATOR

1. Weigh aluminum foil disc sample of 16 mm diameter.
2. Weigh alumina separator coated aluminum disc sample of 16 mm diameter.
3. Subtract weight obtained in step 1, from weight obtained in step 2, this is the weight of alumina in sample.
4. The density of alumina (3.95 g/cm^3) is used to calculate porosity of separator layer.
5. Porous separator layer volume is calculated by multiplying measured thickness of the alumina separator layer with the area of the sample disc.
6. Divide weight obtained in Step 3 by volume calculated in Step 5, to obtain density of porous layer.
7. Subtract the density of porous layer from density of alumina and divide the result by density of alumina to obtain the porosity value of the prepared alumina separator.